

THE PHOTOPRODUCTION OF POSITIVE PIONS FROM HYDROGEN
AT ENERGIES OF 1.1 TO 1.4 GEV

Thesis by
Joseph R. Kilner

In Partial Fulfillment of the Requirements
For the Degree of
Doctor of Philosophy

California Institute of Technology
Pasadena, California

1963

ACKNOWLEDGEMENTS

The interest and guidance of Dr. R. L. Walker during the author's graduate residence have been invaluable. His supervision during the course of this work is greatly appreciated.

The assistance and suggestions of many staff members and graduate students of the Synchrotron Laboratory have been most helpful. Dr. J. O. Maloy has made many valuable contributions to the multipole analysis program.

The active assistance of Dr. R. E. Diebold in accumulating data is deeply appreciated.

L. Loucks and the Synchrotron crew gave excellent support in operating and maintaining the machine and equipment. Special thanks are due E. B. Emery for his maintenance of the liquid hydrogen target. The assistance of all of the synchrotron operators, and especially A. Neubeiser, is appreciated.

Discussions with C. G. Montgomery have been very helpful.

The use of the computing facilities and the assistance of the staffs of both the Western Data Processing Center, University of California at Los Angeles, and the Caltech Computing Center have been invaluable.

The partial financial support of the United States Atomic Energy Commission is gratefully acknowledged.

ABSTRACT

A magnetic spectrometer and counter telescope system was used to detect positive pions photoproduced singly in a liquid hydrogen target. Measurements of the differential cross section were made at mean laboratory photon energies, $k = 1.1, 1.2, 1.3,$ and 1.4 GeV and in the angular range from 5° to 165° in the center-of-momentum system of the pion.

The shape of the angular distribution of the differential cross sections at each value of k is very similar to that of the previously measured distribution at $k = 1.0$ GeV. The angular distributions were integrated to give the total cross sections. The third pion-nucleon "resonance" peak is seen to be very close to $k = 1.0$ GeV. A leveling off of the total cross section at $k = 1.4$ GeV may be due to the fourth "resonance".

The accurate small angle data at $k = 1.1$ and 1.2 GeV permitted a reasonable extrapolation of the differential cross section to the pion-nucleon pole. The value of the pion-nucleon coupling constant, f , was extracted from this extrapolation. The result was

$$f^2 = 0.078 \pm 0.011 .$$

TABLE OF CONTENTS

<u>CHAPTER</u>	<u>TITLE</u>	<u>PAGE</u>
I	INTRODUCTION	1
II	THE EXPERIMENTAL METHOD	3
	A. General	3
	B. The Synchrotron Beam Geometry	5
	C. The Liquid Hydrogen Target	5
	D. The Magnetic Spectrometer	7
	E. The Counter System	7
	F. Particle Selection and Electronics	12
III	THE COUNTING RATES	16
IV	DATA REDUCTION	24
	A. Cross Section Formulas	24
	B. The Calculation of κ	25
V	THE RESULTS	28
VI	ANALYSIS	38
	A. General	38
	B. Moravcsik Polynomial Fitting and the Coupling Constant	38
	C. The 0° and 180° Cross Sections	42
	D. The Total Cross Section	44
	E. Multipole Analysis	44
VII	CONCLUSIONS AND SUGGESTIONS	47
 <u>APPENDIX</u>		
I	COUNTER EFFECIENCIES	49
II	NUCLEAR ABSORPTION	55
III	DECAY AND SCATTERING CORRECTIONS	57
IV	EQUIPMENT CHECKS	77
V	BEAM MONITORING AND THE BREMSSTRAHLUNG SPECTRUM	82
	REFERENCES	86

LIST OF ILLUSTRATIONS

<u>FIGURE</u>	<u>TITLE</u>	<u>PAGE</u>
1.	The Pion Kinematics	4
2.	The Experimental Area	6
3.	The Hydrogen Target and Magnetic Spectrometer	8
4.	Electronics Block Diagram	13
5.	The Background Counting Rates	23
6.	Center of Momentum Angular Distributions	33
7.	The 0° and 180° Cross Sections	43
8.	The Total Cross Section	45
A1.	Cherenkov Counter and Electron Detector Efficiencies	50
A2.	Decay Coordinate System and Parameters	59
A3.	Magnetic Spectrometer Momentum Response	63
A4.	Momentum Response for Muons from the Pion Decay	67
A5.	Multiple Scattering of Pions	76
A6.	Measured and Calculated Spectrometer Response	79
A7.	The Beam Monitor Calibration	83
A8.	The Bremsstrahlung Spectrum	85

LIST OF TABLES

<u>TABLE</u>	<u>TITLE</u>	<u>PAGE</u>
1.	Description of the Counters	11
2.	The Counting Rates	18
3.	The Results	29
4.	Least Squares Coefficients	39
5.	Residues at the Pole and Estimated Points	41
A1.	Parameters for the Decay Correction Program	61
A2.	Multiple Scattering Calculation Parameters	74
A3.	The Spectrometer Acceptance	78

I. INTRODUCTION

The existence of the pi meson was first proposed by Yukawa (1) in 1935. In 1947 Lattes, Occhialini, and Powell (2) discovered the pion in emulsions. Since then a vast amount of experimental and theoretical investigation of the pion and its role in nuclear forces has been done, the pion-nucleon scattering and the pion photoproduction experiments being the most fruitful. Thus far four "resonances" of the pion-nucleon system have been observed. The cross section peaks observed may not actually be resonances but will be referred to as such here. These are (3):

Reso- nance	Mass (MeV)	Width (MeV)	Iso- spin	Angular Momentum	Parity
1	1238	145	3/2	P 3/2	+
2	1512	130	1/2	D 3/2	-
3	1688	140	1/2	F 5/2	+
4	1922	185	3/2	?	?

The first three have been definitely observed in pion photoproduction, and this experiment may detect an indication of the fourth.

At energies in the region of the first resonance and lower, the dispersion theory of Chew, Goldberger, Low, and Nambu (4) is quite successful in fitting the photoproduction data. For lack of a successful theory at higher energies phenomenological methods are used in the analysis of such data. The application of the concepts of Regge poles to the photoproduction analysis problem may prove rewarding at higher energies.

An experiment was planned to measure the angular distributions of π^+ mesons produced in a liquid hydrogen target at pion center of momentum angles from 5° to 165° and at photon energies of 1.1 and 1.2 GeV. The improvement of the synchrotron accelerating system during the course of this experiment made possible an extension to photon energies of 1.3 and 1.4 GeV although the operation at 1.4 GeV was marginal and the statistical accuracy of the data obtained is not very good. An interval of 1.71 to 1.87 GeV in the total c.m. energy is covered in this experiment. At the two higher photon energies the momentum of the pions produced at the forward angles was too high to be analyzed with the largest spectrometer available and the angular distributions are not so complete as at the lower two energies. To a large extent this experiment employed the same apparatus and experimental techniques as used by Dixon (5) and Boyden (6). Thus it is expected that the agreement among these experiments should be quite good.

The angular distributions obtained at all these energies are remarkably similar to the one at $k = 1.0$ GeV. The total cross section decreases markedly to less than $20 \mu\text{b}$ above a photon energy of 1.2 GeV, compared with a total cross section of $55 \mu\text{b}$ at the third resonance peak (very close to 1.0 GeV). The value of the square of the pion-nucleon coupling constant (f^2) measured in this experiment is 0.078 ± 0.011 .

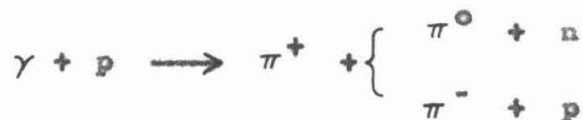
II. THE EXPERIMENTAL METHOD

A. GENERAL

A liquid hydrogen target was irradiated by the photon beam produced by the California Institute of Technology synchrotron. The momentum, p , and angle, θ_{LAB} , of π^+ mesons produced in this target were selected by a magnetic spectrometer and counter telescope system. As is well known, p and θ_{LAB} determine the photon energy, k , (with a width determined by the apparatus) for the reaction



The peak energy of the photon spectrum, E_0 , was chosen so that the pions detected by the counter system were produced only by the above reaction. In particular this proper choice of E_0 eliminated the detection of pions produced in pairs by the processes



and all higher order processes.

The kinematics for single π^+ photoproduction as well as the limiting curve for a π^+ produced in the pair production reactions are given in Figure 1.

In addition to pions, protons and electrons of momentum p were also produced in the forward direction, with the electrons confined to the very forward angles only. The protons were discriminated from the pions by their lower velocity, while the electrons were rejected by

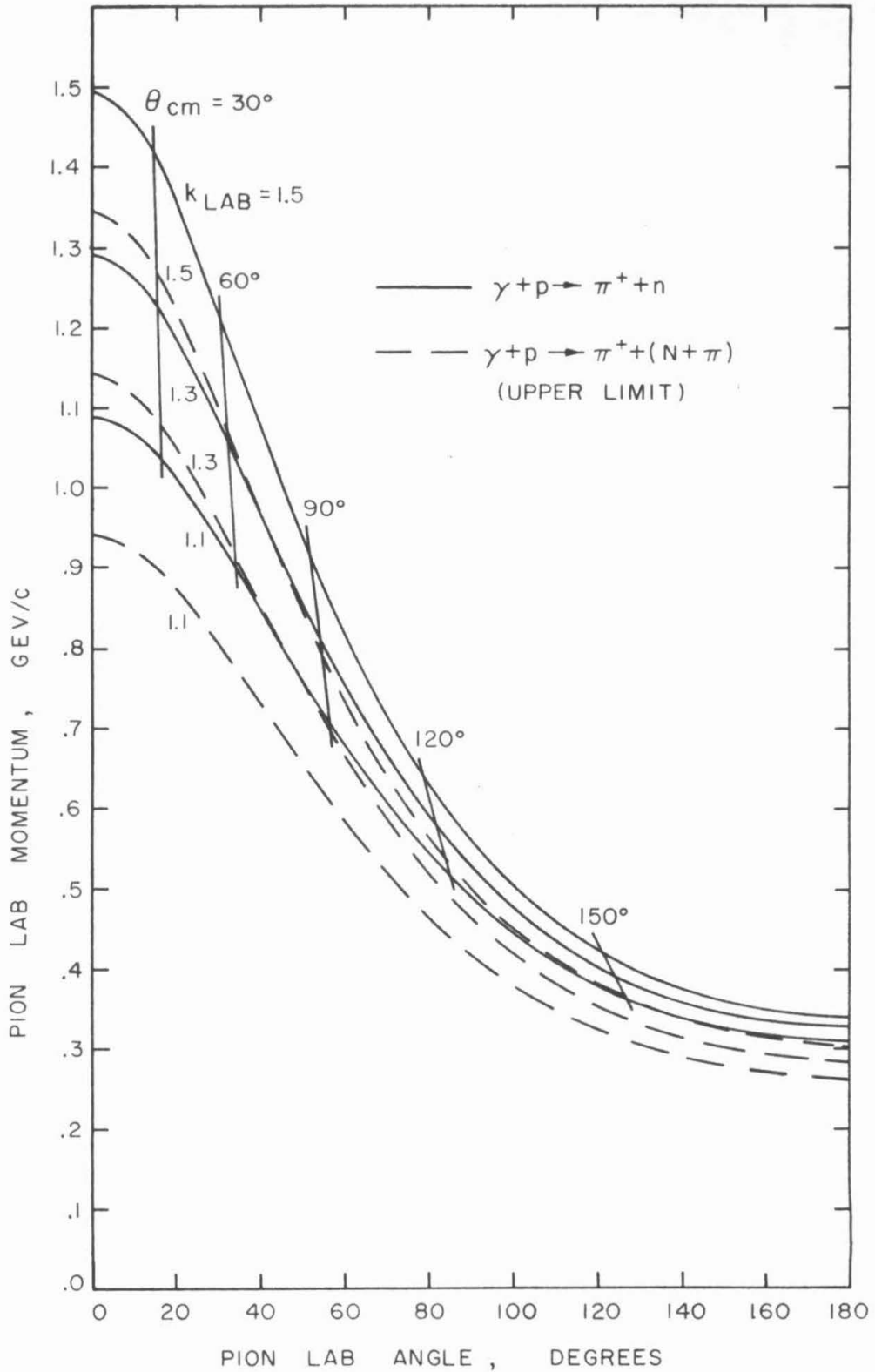


Figure I. The Pion Kinematics

detecting the showers they produced in lead absorbers.

B. THE SYNCHROTRON BEAM GEOMETRY

The overall view of the experimental area and equipment is shown in Figure 2. The photon beam was produced at the radiator inside the synchrotron vacuum chamber, emerged through the primary collimator which fixed the beam size, passed through a lead scraper, then through a sweeping magnet to remove the many (mainly pair-produced) electrons, through a second scraper, struck the liquid hydrogen target, and was finally stopped in the lead block containing the beam monitor. The gas hydrogen target used by T. Chang (7) or various thin targets placed just in front of the sweeping magnet by H. Ruderman (8) were often in the beam while this experiment was in operation. As is discussed in Appendix V the effects of these targets on the bremsstrahlung spectrum may be neglected.

C. THE LIQUID HYDROGEN TARGET

The target of liquid hydrogen was contained in a three inch diameter Mylar cylinder located in a vacuum chamber and surrounded by a series of heat shields cooled by liquid nitrogen. This target was designed by V. Z. Peterson and improved by R. L. Walker. It is a modified version of the one used by Dixon (5) and the same as that used by Boyden (6). The asymmetrical "foghorn"-shaped aluminum shield with Mylar windows shown in Figure 3 is designed to reduce the background from the target structure. When data is taken at small angles (less than 15°) the shield may be rotated 180° from the position shown in Figure 3 (a) to reduce the amount of material the pions must pass

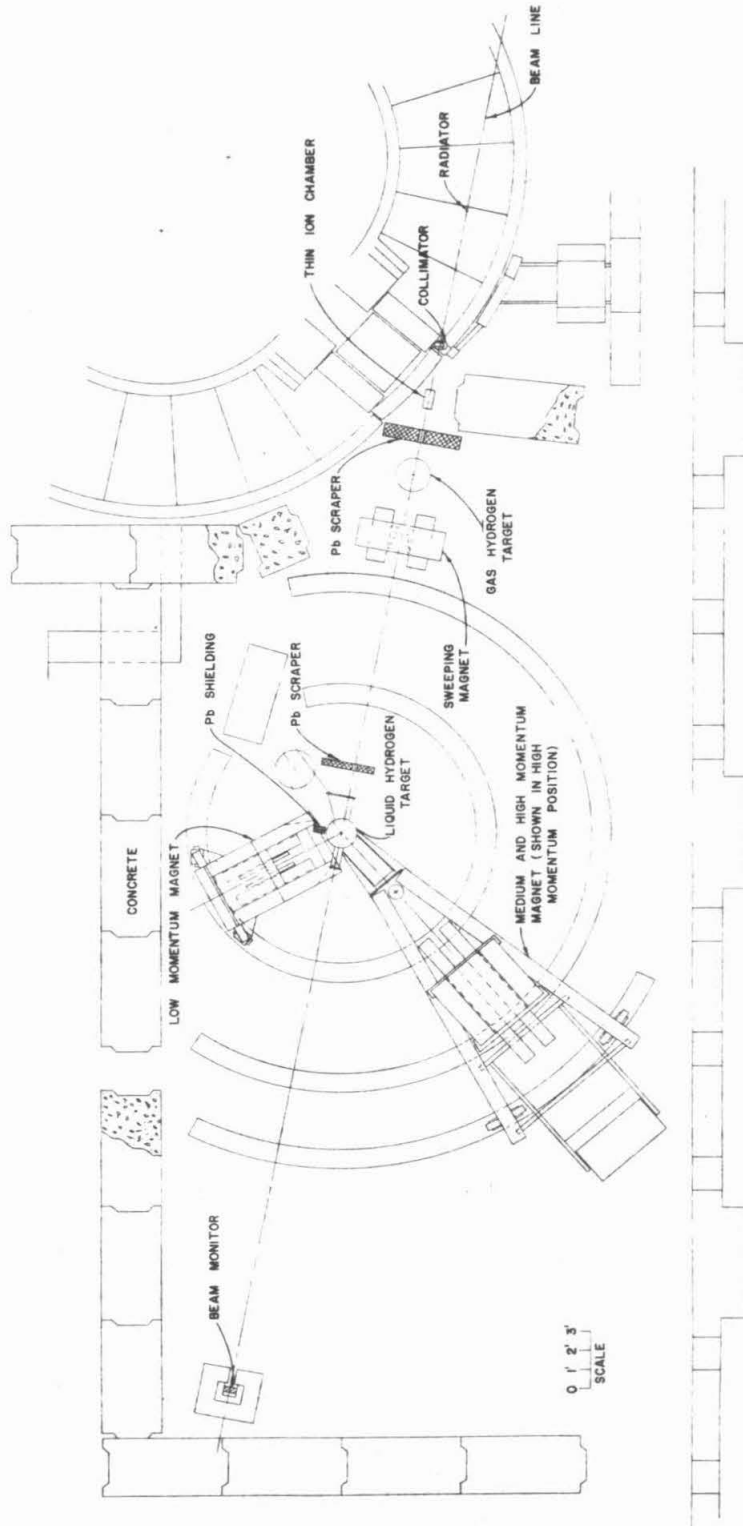


Figure 2. The Experimental Area.

through on emerging from the target.

D. THE MAGNETIC SPECTROMETER

The magnetic spectrometer and counter telescope are shown in both the high and medium energy configurations in Figure 3. An internal report (9) gives a detailed description of this spectrometer and the measurements made to determine its properties. The spectrometer can be easily rotated about the target on the steel tracks shown in Figure 2 and can be set with an error of less than 0.1 degrees. A proton resonance magnetometer was used in adjusting the magnetic field, and the magnet current was regulated to 0.1%. (See Appendix III and Appendix IV for some of the spectrometer properties.)

E. THE COUNTER SYSTEM

The counter system used to detect the particles consisted of five scintillation counters, one lucite Cherenkov counter, and a set of pole face veto counters ("fans") to reject particles scattered from the pole faces. These counters are each described in Table 1 and shown in Figure 3. (See also Appendix III.) Altogether five different configurations of counters and spectrometers were used at the various angles. The Cherenkov counter (\checkmark), C1, C2L, C3, and the "fans" were used in all the configurations except as indicated below. The configurations were:

1. H.E.A2S and H.E.A2L

In the high energy configuration (H.E.) at small angles (less than about 10° in the laboratory), the front aperture counter, A1, could not be used because of the very large number of electrons; thus a rear

Figure 3. The Hydrogen Target and Magnetic Spectrometer

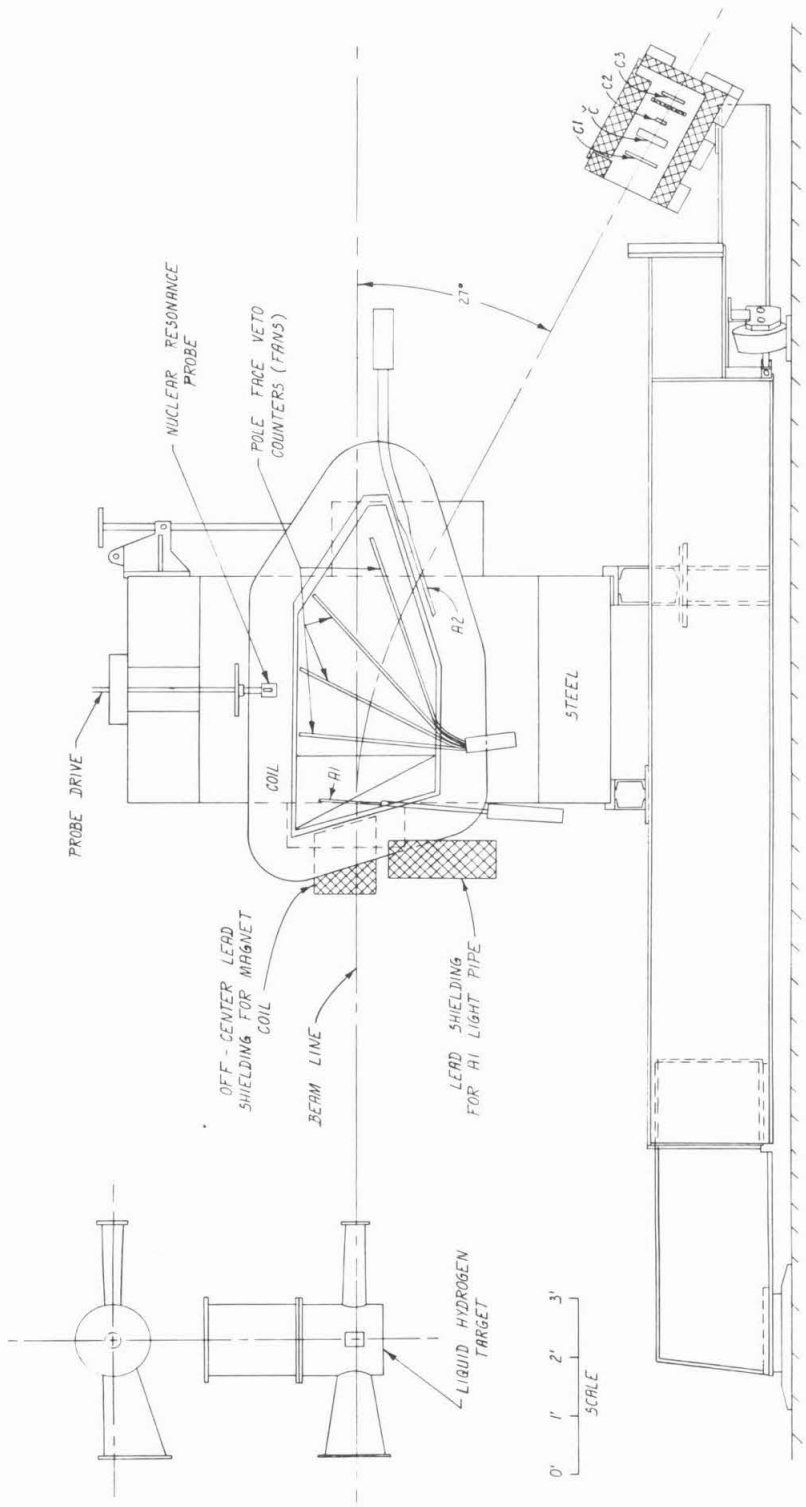
(a) The magnet in the high momentum position is shown at zero degrees.

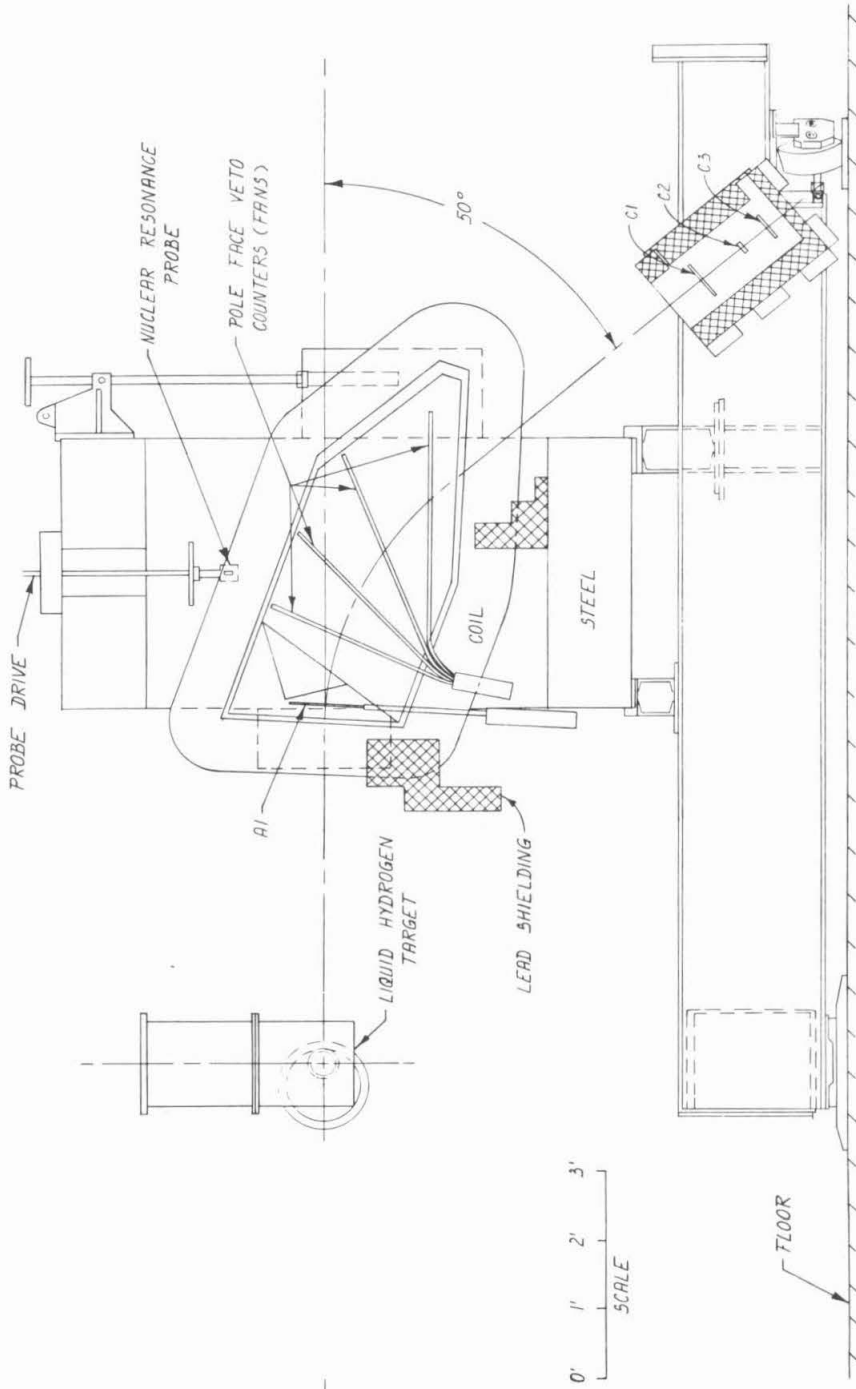
(b) The medium momentum position is shown at 90° .

The bottom portion of the hydrogen target may be rotated 180° from the position shown in (a) to permit operation at laboratory angles less than 15 degrees without a thick portion of the target "horn" in the path of the pions.

Not shown is a four inch thick lead wall placed roughly parallel to the path of the pions in the region between the counter box and the rear aperture of the magnet. This wall served to shield the counters in the counter box from particles produced in the air along the photon beam.

The off center lead shielding in (a) was needed to reduce the number of shower particles entering the magnet gap when the spectrometer was placed at the smallest angles, since the beam then struck the magnet coils close to this gap.





(b)

Table 1
Description of the Counters

Desig.	Type	Size, inches	Use
A1	scint.	12.34 x 3.24 x 0.250	aperture definition and time of flight selection
Fans	scint.	two sets of four rods 1/2 x 3/4 (see Figure 3)	rejection of particles scattered from pole tips
A2	scint.	(A2L) 11.84 x 2.99 x 0.46	aperture definition
		(A2S) 6.00 x 2.99 x 0.46	
C1	scint.	5.75 x 11.0 x 0.787	dE/dx particle selection
C2	scint.	(C2L) 4.75 x 11.0 x 0.787	dE/dx particle selection, time of flight selection, momentum acceptance interval definition, and shower detection
		(C2S) 2.00 x 11.0 x 0.787	
γ C	Cherenkov	6.0 x 11.0 x 1.50	velocity selection
C3	scint.	5.75 x 11.0 x 0.394	dE/dx particle selection and shower detection

aperture counter, A2L or A2S, was used. The small rear aperture counter, A2S, was used at the smallest angles where the larger verticle size of A2L would cause a deterioration of the angular resolution.

2. H.E. and H.E.C2S

In the standard high energy spectrometer configuration used at medium angles, A1 replaces A2. At the larger angles obtainable with the high energy spectrometer ($\sim 50^\circ$) C2S replaced C2L to reduce the momentum acceptance of the spectrometer.

3. M.E.

The Cherenkov counter was removed from the counter box when the medium energy spectrometer was used. A1 and C2S were used in this configuration.

F. PARTICLE SELECTION AND ELECTRONICS

A block diagram of the electronics system is given in Figure 4. Particles traversing the spectrometer system were detected and distinguished by the following four methods:

1. The scintillation counters, A1, A2, C1, C2, and C3 give pulses proportional to the specific ionization, dE/dx .

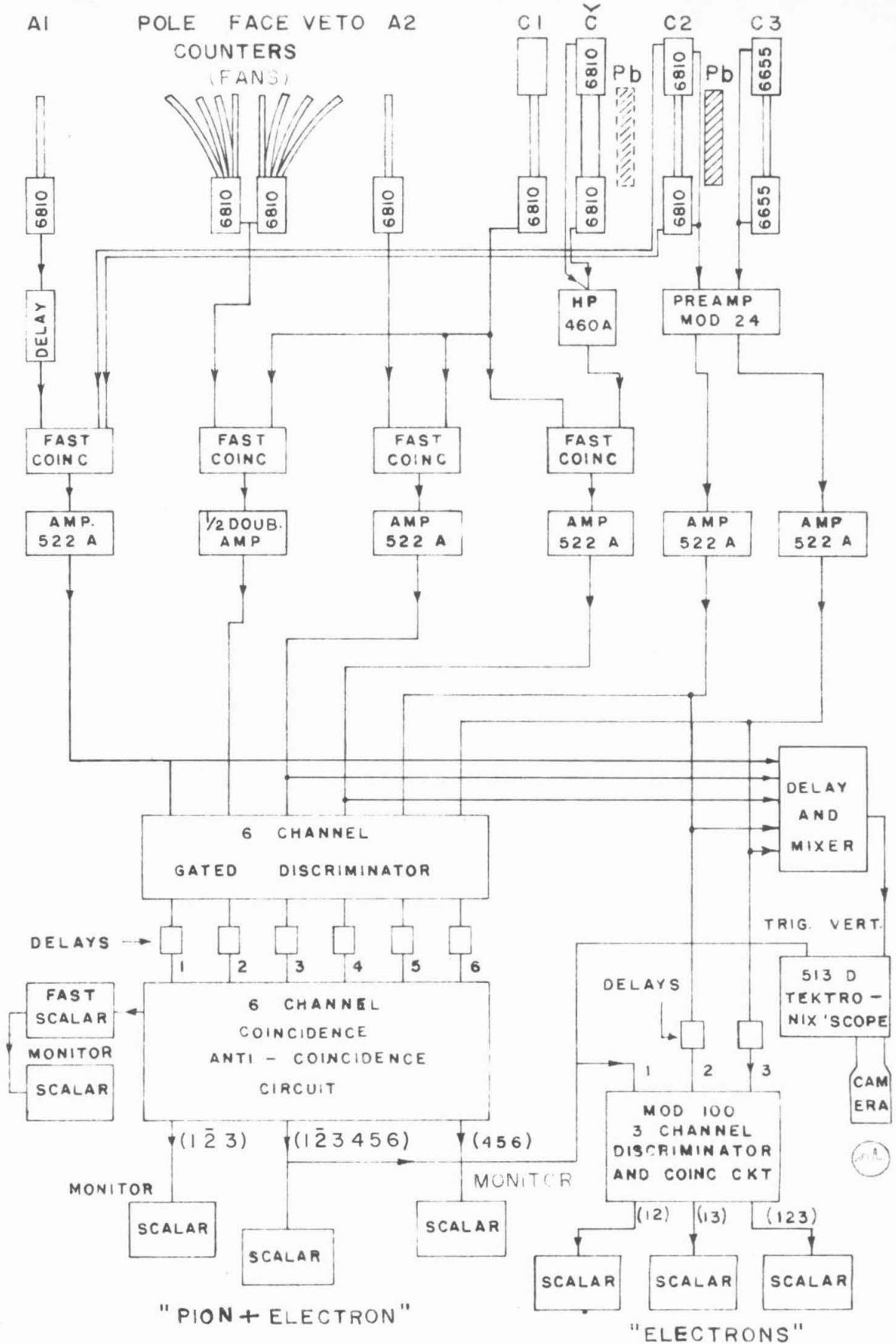
2. The Cherenkov counter which is of the total internal reflection type, gives a pulse only if the particle velocity exceeds about $0.85 c$ (see Appendix I).

3. The A1 - C2 coincidence is a time-of-flight selection system giving an output pulse only if the time the particle takes to go from A1 to C2 is close to some preselected value.

4. Electron showers produced in a $1/2$ " lead converter placed in front of C3 give large pulses in C3. At the smallest angles, where

Figure 4. Electronics Block Diagram

The numbers 6655 and 6810 refer to phototube types. The Hewlett-Packard amplifier is designated by HP. Except for the oscilloscope, all of the other units shown were built at the synchrotron laboratory. The 6 channel coincidence circuit has a resolving time of about a quarter of a micro-second. The fast coincidence circuits, which have adjustable clipping stubs, have resolving times from about 5 to 15 nano-seconds. When the medium energy spectrometer was used the Cherenkov counter was removed and the slow output from C1 was used in place of the C1 \cdot \bar{C} fast coincidence.



large numbers of electrons are present, a second converter placed in front of C2 serves to increase the efficiency for producing large shower pulses (see Appendix I). The use of these methods and the conversion of the various measured counting rates into the actual pion flux will be discussed in the next chapter.

Several experimental tests were made to check the proper functioning of the equipment. These are discussed in Appendix IV.

III. THE COUNTING RATES

In the general case when pions, protons, and electrons were all present three counting rates C, P, and E were measured with and without hydrogen in the target. C and E were taken simultaneously while P required a separate run. These counting rates are defined by the following coincidences:

$$C = (A1 \cdot C2) \cdot \bar{X} \cdot C2 \cdot C3 \cdot \overline{FAN}$$

$$\text{or } (A2 \cdot C1) \cdot \bar{X} \cdot C2 \cdot C3 \cdot \overline{FAN}$$

$$\text{or } (A1 \cdot C2) \cdot C1 \cdot C2 \cdot C3 \cdot \overline{FAN} \quad (\text{M. E. only})$$

$$P = \text{the same as } C \text{ with } \bar{X} \text{ replaced by } \bar{C}$$

$$E = (C \cdot C3^*) \quad (\text{single converter})$$

$$\text{or } (C \cdot C3^*) + (C \cdot C2^*) - (C \cdot C3^* \cdot C2^*) \quad (\text{double converter})$$

where FAN designates the pole face veto counters, a bar over a counter signifies an anticoincidence, and an asterisk means a higher bias is used. Let C_π , C_p , and C_e be respectively the true numbers of pions, protons, and electrons passing through the system. C, P, and E may be written in terms of these as follows:

$$C = \eta_{T\pi} \eta_{\bar{C}\pi} C_\pi + \eta_{Tp} \eta_{\bar{C}p} C_p + \eta_{Te} \eta_{\bar{C}e} C_e$$

$$P = \eta_{T\pi} (1 - \eta_{\bar{C}\pi}) C_\pi + \eta_{Tp} (1 - \eta_{\bar{C}p}) C_p + \eta_{Te}$$

$$(1 - \eta_{\bar{C}e}) C_e$$

$$E = \eta_{T\pi} \eta_{\bar{C}\pi} \eta_{E\pi} C_\pi + \eta_{Tp} \eta_{\bar{C}p} \eta_{Ep} C_p + \eta_{Te}$$

$$\eta_{\bar{C}e} \eta_{Ee} C_e$$

where the η 's are efficiencies (see Appendix I) of the various counters (designated by the first subscript) for the three particles (designated by the second subscript). The time of flight system is designated by T and the electron detection system by E. The T and \check{C} efficiencies for pions and electrons are taken to be identical since their velocities are both above 0.98 c in the forward direction where electrons are present. Since $\eta_{\check{C}\pi}$ is very close to one, P may be approximated by

$$P = \eta_{Tp} (1 - \eta_{\check{C}p}) C_p$$

Solving the above equations for C_π gives

$$C_\pi = \frac{(C - E) - (1 - \eta_{Ee}) C - \eta_{\check{C}p} (1 - \eta_{\check{C}p})^{-1} (\eta_{Ee} - \eta_{Ep}) P}{\eta_{T\pi} \eta_{\check{C}\pi} (\eta_{Ee} - \eta_{E\pi})}$$

When no electrons are present this is

$$C_\pi = \frac{C - \eta_{\check{C}p} (1 - \eta_{\check{C}p})^{-1} P}{\eta_{T\pi} \eta_{\check{C}\pi}}$$

When the medium energy configuration is used (and the Cherenkov counter removed) this becomes

$$C_\pi = \frac{C}{\eta_{T\pi}}$$

All of the measured quantities and the calculated pion fluxes are given in Table 2. The errors on all of the quantities appearing in the equation for C_π are used in calculating the error of C_π .

Some of the data were taken with the fan counters turned off. To

TABLE 2

The Counting Rates

All of the experimentally measured quantities used in calculating the counting rates are given in this table. These quantities are as follows:

PT The point number--the number used throughout the data reduction process is kept here for convenience. The missing numbers were either unused or the data were discarded.

E_0 The bremsstrahlung end point energy in GeV.

p_0 The spectrometer central momentum in GeV/c.

θ_{LAB} The spectrometer angle in degrees.

CONFIG The spectrometer configuration as follows:

M.E. The medium energy spectrometer using the front aperture counter, A1, and the small momentum defining counter C2S.

H.E. The high energy spectrometer using the front aperture counter, A1, and the large momentum defining counter C2L.

The single converter is used unless the double converter, DC, is indicated.

The remaining configurations all refer to changes in the high energy spectrometer configuration. A2S and A2L refer respectively to the small and large rear aperture counters used instead of A1.

C, E, and P These are the counting rates as defined in the text. (An asterisk here indicates an estimated or interpolated counting rate--the backgrounds being given as the fraction of the full target counting rate.)

BIPS The integrated amount of beam intensity used. (See Chapter IV, B, 2.)

- η The η 's refer to the various efficiencies (see Appendix A1). The errors on these four are 0.002, 0.005, 0.005, and 0.002 respectively. In addition $\eta_{C\pi} = 0.9960 \pm .0012$ (H.E. only) and $\eta_{T\pi} = 0.9964 \pm .0014$ were used.
- C_e The electron counting rate in electrons per BIP.
- C_{π}^{**} The pion counting rate in pions per BIP when electron subtraction is included.
- C_{π} The pion counting rate in pions per BIP when it is assumed that no electrons are present. An asterisk after C_{π} indicates that the fan counters were not used when the data was taken and a suitable correction has been made.

In part (b) of the table the columns from $\eta_{E\pi}$ to C_{π}^{**} inclusive have been omitted since the entries are not necessary.

TABLE 2

PT	E ₀	P ₀	θ _{LAB}	CONFIG	C	E	BIPS	P/BIPS	BACKGROUND				C _e	C _π	PI					
									C	E	BIPS	P/BIPS								
2	1.2	1.084	2.7	A2S DC	8681	7146	5276	780/1437	4829	4394	4025	280/1067	.047	.133	.097	.976	.234±.028	.183±.012	* 2	
3	1.2	1.084	2.7	A2S DC	288	229	245	*.45±.05	* 30±.03				.047	.133	.097	.976	.161±.038	* 3		
4	1.2	1.080	4.1	A2S DC	1889	836	5193	754/1662	346	251	2191	80/554	.047	.132	.098	.976	.021±.016	.161±.010	* 4	
5	1.2	1.080	4.1	A2S	344	139	775	141/295	* 21±.03				.047	.093	.078	.929	.195±.024	* 5		
6	1.2	1.078	5.4	A2L	3211	656	6512	1338/1459	238	71	2436	245/681	.047	.093	.078	.929	.040±.017	.315±.012	* 6	
7	1.2	1.078	5.4	A2S DC	756	161	3203	340/772	55	20	1278	69/560	.047	.132	.099	.976	.012±.015	.160±.011	* 7	
8	1.2	1.072	8.1	A2L	3328	323	8493	1648/2069	118	10	2569	188/961	.046	.092	.080	.929	.003±.013	.302±.010	.305±.008*	8
9	1.2	1.072	8.1	H.E.	202	22	337	94/183	* 12±.02				.046	.092	.080	.929	.499±.049	.509±.044	9	
10	1.2	1.062	10.9	H.E.	3559	283	5544	547/1365	111	13	1519	65/565	.045	.091	.083	.928	-.011±.021	.571±.015	.560±.013	10
11	1.2	1.062	10.9	A2L	132	13	333	136/231	* 10±.02				.045	.091	.083	.928	.004±.055	.315±.042	.320±.036*	11
12	1.2	1.036	16.2	H.E.	4096	378	6382	485/1819	115	6	2767	41/701	.043	.088	.090	.927	.005±.018	.590±.013	.595±.011	12
13	1.2	.975	25.0	H.E.	2820	4854	126/1112		40	1318	3/578		.039				.550±.012	13		
14	1.2	.895	34.3	H.E.	1462	3929	26/935		14	915	0		.033				.359±.011	14		
15	1.2	.803	44.6	H.E.	936	5446	1/618		* 0.42±.01				.029				.166±.006	15		
16	1.2	.716	54.6	H.E.	393	4629	1/654		* 0.45±.01				.028				.082±.004	16		
17	1.2	.716	54.6	C2S	98	2669	0		* 0.45±.01								.035±.004	17		
18	1.2	.603	70.0	M.E.	286	3537	0		11	3050	0						.078±.005	18		
19	1.2	.509	85.7	M.E.	327	3969	0		22	3158	0						.076±.005	19		
20	1.2	.427	104.4	M.E.	323	3736	0		13	2633	0						.082±.005	20		
21	1.3	.427	104.4	M.E.	317	4088	0		9	1855	0						.073±.005	21		
22	1.2	.386	117.2	M.E.	241	4116	0		15	2038	0						.051±.004	22		
23	1.3	.363	126.5	M.E.	298	4979	0		4	1446	0						.057±.004	23		
24	1.3	.323	152.1	M.E.	175	4320	0		10	2130	0						.036±.003	24		
25	1.3	1.183	3.1	A2S DC	1265	812	2861	168/534	196	158	772	62/337	.055	.149	.078	.977	.054±.026	.113±.013	25	
26	1.3	1.183	3.1	A2S DC	1287	840	2418	166/467	* 27±.03				.055	.149	.078	.977	.012±.012	.131±.012	* 26	
27	1.3	1.179	5.2	A2L	769	124	2077	180/282	106	27	1242	121/500	.055	.102	.052	.935	.012±.024	.252±.018	27	
28	1.3	1.179	5.2	A2S	71	14	492	18/79	* 15±.03				.055	.102	.052	.935	.098±.019	* 0.98±.019	28	
29	1.3	1.160	10.6	A2L	651	69	2360	735/1254	19	1	827	28/266	.053	.101	.057	.934	.004±.019	.221±.014	.225±.012	29
30	1.3	1.160	10.6	A2S	104	13	817	62/249	* 10±.02				.053	.101	.057	.934	.099±.015	.103±.013	30	
31	1.3	1.160	10.6	A2L DC	438	62	1600	241/451	* 10±.02				.053	.146	.082	.977	.200±.015	.221±.014	31	
32	1.3	1.130	16.0	H.E.	887	82	1936	213/499	24	3	1177	16/340	.051	.098	.065	.932	-.003±.025	.423±.019	.420±.016	32
33	1.3	1.130	16.0	A2L	140	20	463	85/152	* .05±.02				.051	.098	.065	.932	.231±.028	.248±.025	33	
34	1.3	1.062	24.5	H.E.	561	1773	113/567		7	556	3/185		.045				.297±.014	34		

(d)

PT	E ₀	p ₀	θ _{LAB}	CONFIG	C	E	HIPS	P/BIPS	C	E	BIPS	P/BIPS	η _{EP}	C _π	PT
35	1.3	.973	33.7	H.E.	224	1319	8/213		6	.779	1/582		.039	.162±.012	35
36	1.3	.870	43.8	H.E.	97	1672	0/363		*	.042±.01				.057±.006	36
37	1.3	.870	43.8	H.E.	35	448	0		*	.042±.01				.076±.013*	37
38	1.3	.758	55.2	H.E.	70	1916	0		*	.046±.01				.035±.004	38
40	1.3	.632	70.3	M.E.	198	3830	0		9	3231	0			.049±.004	40
41	1.3	.541	84.0	M.E.	167	5093	0		*	.065±.02				.031±.003	41
42	1.3	.450	102.7	M.E.	221	4996	0		9	2103	0			.040±.003	42
43	1.4	.450	102.7	M.E.	171	4090	0		5	1710	0			.039±.004	43
44	1.3	.400	117.2	M.E.	118	3359	0		5	1513	0			.032±.004	44
45	1.4	.360	133.4	M.E.	196	5405	0		8	1866	0			.032±.003	45
46	1.4	.332	151.3	M.E.	82	4007	0		*	.12±.04				.018±.002	46
50	1.4	1.191	15.6	H.E.	748	2848	74/292		10	416	5/163		.056	.227±.013	50
51	1.4	1.149	23.8	H.E.	540	1857	195/566		11	699	2/187		.052	.259±.014	51
53	1.4	1.050	32.8	H.E.	463	3437	48/702		7	1249	2/191		.045	.127±.007	53
54	1.4	1.050	32.8	C2S	135	2273	21/236		*	.042±.01			.045	.053±.005	54
55	1.4	.934	42.6	H.E.	92	1785	6/649		*	.042±.01			.036	.049±.005	55
57	1.4	.936	42.6	C2S	33	1610	*.004±.002		*	.042±.01			.036	.020±.004	57
58	1.4	.812	53.9	H.E.	57	1993	0/543		*	.046±.01				.028±.004	58
59	1.4	.812	53.9	C2S	62	3986	0		*	.046±.01				.015±.002	59
60	1.4	.610	76.9	M.E.	168	4518	0		*	.06±.02				.035±.003	60
61	1.4	.472	101.2	M.E.	140	3864	0		9	2092	0			.032±.003	61
62	1.4	.416	115.8	M.E.	129	3973	0		2	1130	0			.031±.003	62
63	1.5	.343	150.5	M.E.	13	742	0		*	.12±.04				.016±.005	63
65	1.5	1.165	26.1	H.E.	193	1482	25/392		2	409	1/150		.054	.123±.010	65
66	1.5	1.127	32.0	H.E.	171	1436	33/418		5	924	2/169		.051	.111±.010	66
67	1.5	1.002	41.6	H.E.	178	3807	4/206		*	.042±.01			.041	.044±.004	67
68	1.5	.866	52.7	H.E.	38	1411	0		*	.046±.01				.026±.004	68
69	1.5	.603	80.9	M.E.	54	1583	0		*	.065±.02				.032±.005	69
70	1.5	.493	99.7	M.E.	47	1504	0		*	.08±.03				.029±.005	70
71	1.5	.432	114.4	M.E.	29	1481	0		*	.09±.03				.018±.004	71

(b)

correct for this the fraction of counted particles (the unscattered ones as well as those scattered from the pole faces) passing through the fans was measured (at the spectrometer central momentum, $p_0 = 1.036$ GeV/c, $\theta_{\text{LAB}} = 16.0$, and $E_0 = 1.2$ GeV) and found to be $0.043 \pm .008$. It is assumed that this fraction may be subtracted from all the counting rates taken with the fans off to correct for this condition.

The background (empty target) counting rates were not always measured but could be estimated using the curve given in Figure 5 obtained from the measured points.

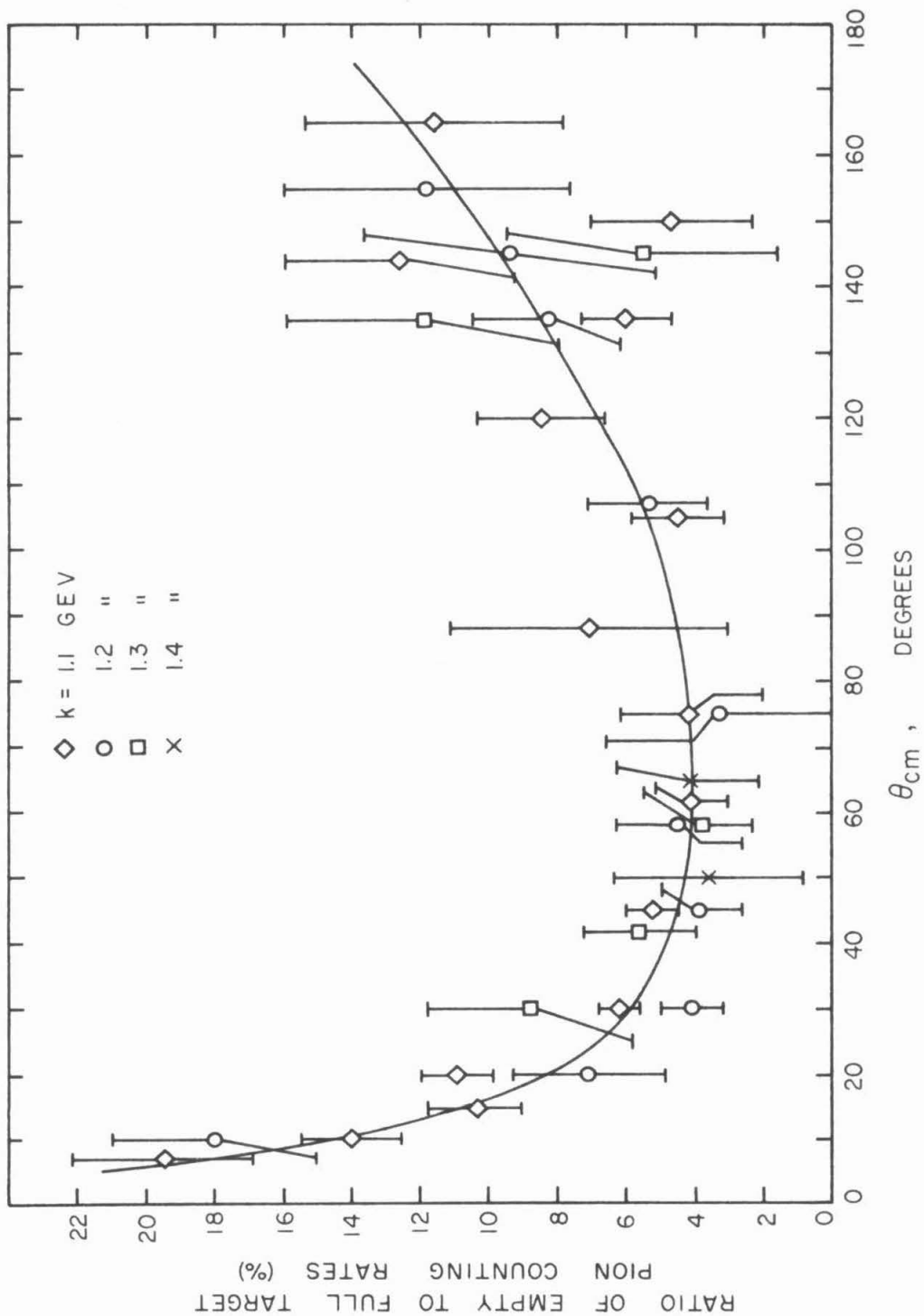


Figure 5. The Background Counting Rates

IV. DATA REDUCTION

A. CROSS SECTION FORMULAS

The observed pion counting rate, C_π , may be expressed in terms of geometrical and kinematical quantities and the cross section, $\sigma(k, \theta)$.

$$C_\pi = \iiint \iiint \iiint \sigma(k, \theta) R A_\pi N_H N(k) n(x, y) \frac{\partial \Omega}{\partial \Omega_L} dx dy dz dk d\Omega_L$$

where

- R = correction for the pion decay including the muon background (see Appendix III)
- A_π = correction for the pion absorption (see Appendix II)
- N_H = the effective number of hydrogen nuclei per unit volume
- $N(k)dk$ = the number of photons per BIP with energy k in the interval dk
- $n(x, y)$ = the relative beam intensity at the target
- $\frac{\partial \Omega}{\partial \Omega_L}$ = the transformation from c.m. to lab. solid angle
- $d\Omega_L$ = laboratory solid angle increment.

The limits on these integrations are functions of the variables in the integrand making the detailed integration quite complicated. $\sigma(k, \theta)$ is the unknown quantity that is to be measured in this experiment, but only the average value over the limits of these integrations may be obtained. Actually many of the quantities in the integrand are nearly

constant and can be replaced by their average values. The following simplified equations containing average and integrated quantities may be used.

$$\sigma(k, \theta) = C_{\pi} / \kappa$$

where

$$\kappa = RA_{\pi} N_H \frac{W \bar{B}(k, E_0)}{\bar{k} E_0} \bar{l} G(\Delta\Omega \frac{\Delta P}{P_0}) P_0$$

W = a normalization factor (see section B)

$\bar{B}(k, E_0)$ = the average value of the photon spectrum (see section B)

\bar{k} = the mean photon energy

\bar{l} = the mean path length for the photon beam through the target

G = the average value of $\frac{\partial \Omega}{\partial \Omega_L} \frac{\partial k}{\partial p}$

$\Delta\Omega$ = the average solid angle of the spectrometer

$\frac{\Delta P}{P_0}$ = the momentum dispersion of the spectrometer

P_0 = the spectrometer central momentum

B. THE CALCULATION OF κ

1. Hydrogen Density

The liquid hydrogen target is operated at 1/2 psi above atmospheric pressure at its boiling point, which corresponds to a density of 0.0707 g/cc. The background runs were taken with hydrogen

gas at the same temperature and pressure instead of liquid in the target. The gas density is 0.0015 g/cc. The effective hydrogen density (for the full target minus background runs) is thus

$$\rho_H = 0.0707 - 0.0015 = 0.0692 \text{ g/cc.}$$

Using 1.008 for the atomic weight, M , and 6.024×10^{23} for Avogadro's number, N_0 , the density of hydrogen nuclei

$$N_H = \frac{\rho_H N_0}{M} = 0.4136 \times 10^{23} \text{ nuclei/cc}$$

is obtained.

2. The Photon Population

In the equation for κ , the integral of $N(k)$ over the acceptance region of the spectrometer has been expressed in terms of

$$B(k, E_0) = \frac{E_0}{W} k N(k)$$

where W is a normalization factor such that

$$\int_0^{E_0} B(k, E_0) dk = E_0$$

The measurements of W and $B(k, E_0)$ are discussed in Appendix V.

$\bar{B}(k, E_0)$ and \bar{k} were calculated using a simple computer program which averaged the photon spectrum, $B(k, E_0)$, over the momentum resolution function of the magnet. The resolution functions used were taken from the results of the decay correction calculation (see Appendix III) except the one for the high energy configuration using A1 and C2L which was taken from the magnet report (9).

3. The Effective Target Length, \bar{l}

A computer program written by J. Boyden (6) was used to average the target thickness weighted by the beam density. This program contained within it the spatial distribution of the beam, $n(x, y)$, (measured by J. Boyden) which has a slight energy dependence, and evaluated the integral

$$\bar{l} = \iiint n(x, y) dx dy dz$$

where the limits are determined by the target size and position.

The remaining non-kinematical quantities are discussed in the appendices: R in III, A_{π} in II, and the spectrometer acceptance,

$$\frac{\Delta P}{P_0} \Delta \Omega, \text{ in IV.}$$

The values of κ and each of its separate factors are given in Table 3 in the next chapter.

V. THE RESULTS

The differential cross-section and all the quantities used in calculating it are given in Table 3. Also given is the differential cross section averaged over all the configurations used at a particular θ and k . This averaged value has also been interpolated to k values of 1.1, 1.2, 1.3, and 1.39 GeV for convenience in handling the data. The differential cross section for each of these k values is plotted in Figure 6, along with a curve which will be discussed in the next chapter. In Table 3 and Figure 6 only those statistical errors which arise from the counting rate and efficiency measurements are given. Most of the systematic errors are estimated to be only a few per cent (see Appendix IV). As an indication of the effects of an error in E_0 , the change in the calculated differential cross section, due to a 2% increase in E_0 has been computed and is given in Table 3.

TABLE 3
The Results

All the quantities used in calculating the cross sections from the counting rates are given here. The hydrogen density $N_H = 0.4136 \times 10^{23}$ nuclei/cc was used for all points.

PT	The point number as in Table 2.
θ_{LAB}	The spectrometer angle in degrees.
θ	The pion center-of-momentum angle in degrees.
E_0	The bremsstrahlung end point energy in GeV.
p_0	The spectrometer central momentum in GeV/c.
p_0^s	The pion momentum at the source corresponding to p_0 in GeV/c.
\bar{E}	The mean photon energy in GeV.
R	The decay correction.
A_π	The absorption correction.
ACC	The spectrometer acceptance, $(\Delta\Omega)(\Delta p/p_0)$.
\bar{l}	The effective length of the hydrogen target in cm.
\bar{B}	The mean value of the photon spectrum, $B(k, E_0)$, in the range used.
G	$(\partial k / \partial p) (\partial \Omega / \partial \Omega_{LAB})$
W	The energy per BIP in GeV/BIP.
κ	$\sigma = C_\pi / \kappa$ (See text)
C_π	The pion counting rate in pions/BIP taken from Table 2.
Δ	The fractional change in the calculated value of σ when using a value of E_0 2% larger than the one shown in this table.

σ

The differential cross section in $\mu\text{b/SR}$.

$\bar{\sigma}$

The differential cross section in $\mu\text{b/SR}$ averaged over the various configurations used and interpolated (or extrapolated) to the values of k shown.

TABLE 3

PT	θ_{LAB}	θ	E_0	P_0	P_0^s	\bar{K}	R	A	$ACC \times 10^{-4}$	\bar{I}	\bar{B}	G	$M \times 10^{29}$	$K \times 10^{29}$	$C\pi$	Δ	σ	$\bar{\sigma}$
2	2.7	5.0	1.2	1.084	1.088	1.100	.948	.820	.54	7.262	.850	3.38	.870	.259	.183±.012	-0.0004	7.08±.46	1.100
3	2.7	5.0	1.2	1.084	1.088	1.100	.948	.820	.54	7.262	.850	3.38	.874	.260	.161±.038	-0.0004	6.2 ±1.5	7.00±.44
4	4.1	7.5	1.2	1.080	1.084	1.098	.948	.820	.54	7.262	.852	3.38	.871	.259	.161±.010	.0006	6.23±.39	
5	4.1	7.5	1.2	1.080	1.084	1.098	.948	.861	.54	7.262	.852	3.38	.872	.272	.195±.024	.0006	7.18±.88	6.35±.36
6	5.4	10.0	1.2	1.078	1.082	1.098	.952	.861	1.08	7.262	.852	3.38	.867	.254	.315±.012	.0005	5.80±.22	
7	5.4	10.0	1.2	1.078	1.082	1.098	.974	.820	.54	7.262	.851	3.38	.871	.258	.160±.011	.0000	6.21±.43	5.87±.20
8	8.1	15.0	1.2	1.072	1.076	1.099	.952	.861	1.08	7.262	.851	3.38	.864	.537	.305±.008	.0001	5.68±.15	
9	8.1	15.0	1.2	1.072	1.076	1.096	.946	.861	1.95	7.262	.853	3.38	.867	.974	.509±.044	.0011	5.23±.45	5.62±.14
10	10.9	20.0	1.2	1.062	1.066	1.096	.946	.861	1.95	7.262	.853	3.38	.866	.964	.560±.013	.0009	5.81±.13	
11	10.9	20.0	1.2	1.062	1.066	1.099	.952	.861	1.08	7.262	.850	3.38	.864	.532	.320±.036	-0.0003	6.02±.68	5.76±.13
12	16.2	29.5	1.2	1.036	1.040	1.096	.945	.861	1.95	7.262	.852	3.38	.867	.938	.595±.011	.0004	6.35±.12	6.28±.12
13	25.0	44.5	1.2	.975	.979	1.095	.939	.861	1.95	7.262	.850	3.37	.877	.884	.550±.012	-0.0007	6.22±.14	6.09±.14
14	34.3	55.5	1.2	.895	.900	1.094	.931	.861	1.95	7.262	.847	3.36	.876	.800	.359±.011	-0.0027	4.49±.14	4.35±.14
15	44.6	74.4	1.2	.803	.807	1.092	.921	.861	1.95	7.262	.841	3.34	.876	.702	.166±.006	-0.0074	2.36±.09	2.24±.09
16	54.6	87.5	1.2	.716	.721	1.090	.908	.861	1.95	7.262	.830	3.32	.876	.606	.082±.004	-0.0154	1.35±.07	
17	54.6	87.5	1.2	.716	.721	1.090	.906	.861	.87	7.262	.865	3.32	.891	.284	.035±.004	.0063	1.24±.13	1.27±.06
18	70.0	105.1	1.2	.603	.608	1.090	.938	.907	2.75	7.262	.862	3.29	.893	.821	.078±.005	.0062	.94±.06	.82±.06
19	85.7	120.0	1.2	.509	.513	1.087	.928	.907	2.75	7.262	.862	3.23	.894	.675	.076±.005	.0059	1.12±.07	1.04±.07
20	104.4	135.1	1.2	.427	.432	1.088	.911	.907	2.75	7.262	.854	3.16	.895	.539	.082±.005	.0008	1.52±.09	
21	104.4	135.1	1.3	.427	.432	1.090	.927	.907	2.75	7.266	.886	3.16	.891	.523	.073±.005	.0179	1.40±.09	1.39±.06
22	117.2	144.1	1.2	.386	.391	1.087	.899	.907	2.75	7.262	.850	3.10	.896	.471	.051±.004	-0.0022	1.09±.09	1.04±.09
23	126.5	150.1	1.3	.363	.368	1.089	.902	.907	2.75	7.266	.886	3.06	.892	.420	.057±.004	.0177	1.37±.09	1.33±.09
24	152.1	165.0	1.3	.323	.327	1.040	.880	.907	2.75	7.266	.885	2.98	.892	.352	.036±.003	.0174	1.02±.10	.97±.10
25	3.1	6.0	1.3	1.183	1.187	1.199	.955	.820	.54	7.266	.840	3.59	.880	.256	.113±.013	-0.0063	4.42±.51	K = 1.200
26	3.1	6.0	1.3	1.183	1.187	1.199	.955	.820	.54	7.266	.840	3.59	.880	.256	.131±.012	-0.0063	5.12±.47	4.76±.32
27	5.2	10.0	1.3	1.179	1.183	1.199	.949	.861	1.08	7.266	.841	3.60	.880	.534	.252±.018	-0.0062	4.72±.34	
28	5.2	10.0	1.3	1.179	1.183	1.199	.955	.861	.54	7.266	.840	3.60	.880	.268	.098±.019	-0.0066	3.66±.71	4.50±.31
29	10.6	20.0	1.3	1.160	1.164	1.198	.949	.861	1.08	7.266	.840	3.59	.880	.525	.225±.012	-0.0067	4.29±.23	
30	10.6	20.0	1.3	1.160	1.164	1.199	.953	.861	.54	7.266	.839	3.59	.880	.262	.103±.013	-0.0072	3.93±.50	
31	10.6	20.0	1.3	1.160	1.164	1.198	.949	.820	1.08	7.266	.840	3.59	.879	.499	.221±.014	-0.0067	4.23±.28	4.21±.17
32	16.0	30.0	1.3	1.130	1.134	1.196	.946	.861	1.95	7.266	.839	3.60	.879	.921	.420±.016	-0.0072	4.56±.17	
33	16.0	30.0	1.3	1.130	1.134	1.200	.949	.861	1.08	7.266	.836	3.60	.878	.507	.248±.025	-0.0093	4.89±.49	4.56±.17
34	24.5	45.0	1.3	1.062	1.067	1.197	.942	.861	1.95	7.266	.833	3.59	.861	.857	.297±.014	-0.0120	3.45±.16	3.41±.16

(a)

$\frac{\omega}{\Gamma}$

PT	θ_{LAB}	θ	E_0	P_0	P_0^s	\bar{K}	R	A_{π}	ACC $\times 10^{-4}$	\bar{I}	\bar{B}	G	W $\times 10^9$	K $\times 10^{-29}$	C_{π}	Δ	σ	$\bar{\sigma}$	
35	33.7	60.0	1.3	.973	.978	1.196	.935	.861	1.95	7.266	.824	3.58	.879	.768	.162±.012	-.0190	2.11±.15	2.07±.15	
36	43.8	75.0	1.3	.870	.874	1.195	.924	.861	1.95	7.266	.808	3.57	.879	.663	.057±.006	-.0315	.85±.09	.88±.08	
37	43.8	75.0	1.3	.870	.874	1.195	.924	.861	1.95	7.266	.808	3.57	.879	.663	.076±.013	-.0315	1.15±.20	.62±.08	
38	52.2	90.0	1.3	.758	.763	1.191	.910	.861	1.95	7.266	.780	3.55	.878	.547	.035±.004	-.0621	.64±.08	.63±.05	
40	70.3	107.0	1.3	.632	.636	1.188	.938	.907	2.75	7.266	.856	3.51	.886	.764	.049±.004	.0024	.64±.05	.63±.05	
41	84.0	120.0	1.3	.541	.546	1.187	.929	.907	2.75	7.266	.851	3.46	.887	.637	.031±.003	-.0006	.48±.04	.48±.04	
42	102.7	135.1	1.3	.450	.454	1.186	.913	.907	2.75	7.266	.841	3.38	.888	.505	.040±.003	-.0082	.79±.07	.79±.07	
43	107.7	135.1	1.4	.450	.454	1.188	.928	.907	2.75	7.270	.884	3.38	.885	4.98	.039±.004	-.0174	.78±.07	.76±.05	
44	117.2	145.0	1.3	.400	.404	1.183	.900	.907	2.75	7.266	.835	3.31	.888	.431	.032±.004	-.0126	.74±.08	.74±.08	
45	133.4	155.0	1.4	.360	.365	1.183	.898	.907	2.75	7.270	.884	3.24	.886	.372	.032±.003	.0171	.86±.08	.84±.08	
46	151.3	165.0	1.4	.332	.337	1.179	.883	.907	2.75	7.270	.884	3.17	.885	.330	.018±.002	.0170	.54±.07	.52±.07	
$K = 1.300$																			
50	15.6	30.0	1.4	1.191	1.231	1.298	.947	.655	1.95	7.270	.820	3.82	.873	.652	.227±.013	-.0207	3.48±.24	3.47±.24	
51	23.8	45.0	1.4	1.149	1.154	1.295	.945	.861	1.95	7.270	.819	3.81	.874	.825	.259±.014	-.0224	3.14±.17	3.12±.17	
53	32.8	60.0	1.4	1.050	1.055	1.293	.940	.861	1.95	7.270	.808	3.80	.872	.738	.127±.007	-.0306	1.73±.09	1.73±.09	
54	32.8	60.0	1.4	1.050	1.055	1.295	.939	.861	.87	7.270	.848	3.80	.875	.343	.053±.005	-.0020	1.55±.15	1.66±.08	
55	42.6	74.8	1.4	.934	.938	1.287	.930	.861	1.95	7.270	.802	3.77	.871	.642	.049±.005	-.0434	.77±.08	.77±.08	
57	42.6	74.9	1.4	.936	.940	1.294	.930	.861	.87	7.270	.848	3.76	.871	.301	.020±.004	-.0018	.65±.12	.73±.07	
58	53.9	90.2	1.4	.812	.817	1.287	.915	.861	1.95	7.270	.755	3.76	.871	.516	.028±.004	-.0651	.53±.07	.53±.07	
59	53.9	90.2	1.4	.812	.817	1.294	.915	.861	.87	7.270	.845	3.76	.875	.256	.015±.003	-.0040	.59±.08	.56±.05	
60	76.9	115.0	1.4	.610	.614	1.284	.934	.907	2.75	7.270	.845	3.70	.877	.651	.035±.003	-.0042	.54±.05	.54±.05	
61	101.2	135.0	1.4	.472	.475	1.281	.915	.907	2.75	7.270	.829	3.60	.879	.473	.032±.003	-.0165	.68±.07	.67±.07	
62	115.8	145.0	1.4	.416	.421	1.260	.904	.907	2.75	7.270	.814	3.53	.880	.399	.031±.003	-.0255	.77±.08	.74±.08	
63	150.5	165.0	1.5	.343	.347	1.266	.884	.907	2.75	7.274	.879	3.40	.849	.299	.016±.005	.0147	.52±.13	.52±.13	
$K = 1.350$																			
65	26.1	50.0	1.5	1.165	1.207	1.393	.945	.655	1.95	7.274	.798	4.02	.836	.543	.123±.010	-.0334	2.27±.21	2.27±.21	
66	32.0	60.0	1.5	1.127	1.132	1.390	.942	.861	1.95	7.274	.789	4.01	.836	.681	.111±.010	-.0457	1.63±.14	1.63±.14	
67	41.6	74.9	1.5	1.002	1.006	1.387	.934	.861	1.95	7.274	.767	4.00	.836	.584	.044±.004	-.0602	.76±.06	.76±.06	
68	52.7	90.0	1.5	.866	.871	1.382	.920	.861	1.95	7.274	.728	3.98	.836	.471	.026±.004	-.0600	.55±.09	.55±.09	
69	80.9	120.0	1.5	.603	.607	1.381	.932	.907	2.75	7.274	.832	3.90	.845	.558	.032±.005	-.0138	.58±.09	.58±.09	
70	99.7	135.1	1.5	.493	.497	1.377	.918	.907	2.75	7.274	.813	3.82	.845	.431	.029±.005	-.0269	.67±.11	.67±.11	
71	114.4	145.1	1.5	.432	.437	1.375	.905	.907	2.75	7.274	.793	3.75	.845	.358	.018±.004	-.0375	.50±.10	.50±.10	

(b)

Figure 6. Center of Momentum Angular Distributions of Pions from the Reaction $\gamma + p \rightarrow \pi^+ + n$ at the Following Laboratory Photon Energies, k :

- (a) $k = 1.1$ GeV
- (b) $k = 1.2$ GeV
- (c) $k = 1.3$ GeV
- (d) $k = 1.39$ GeV

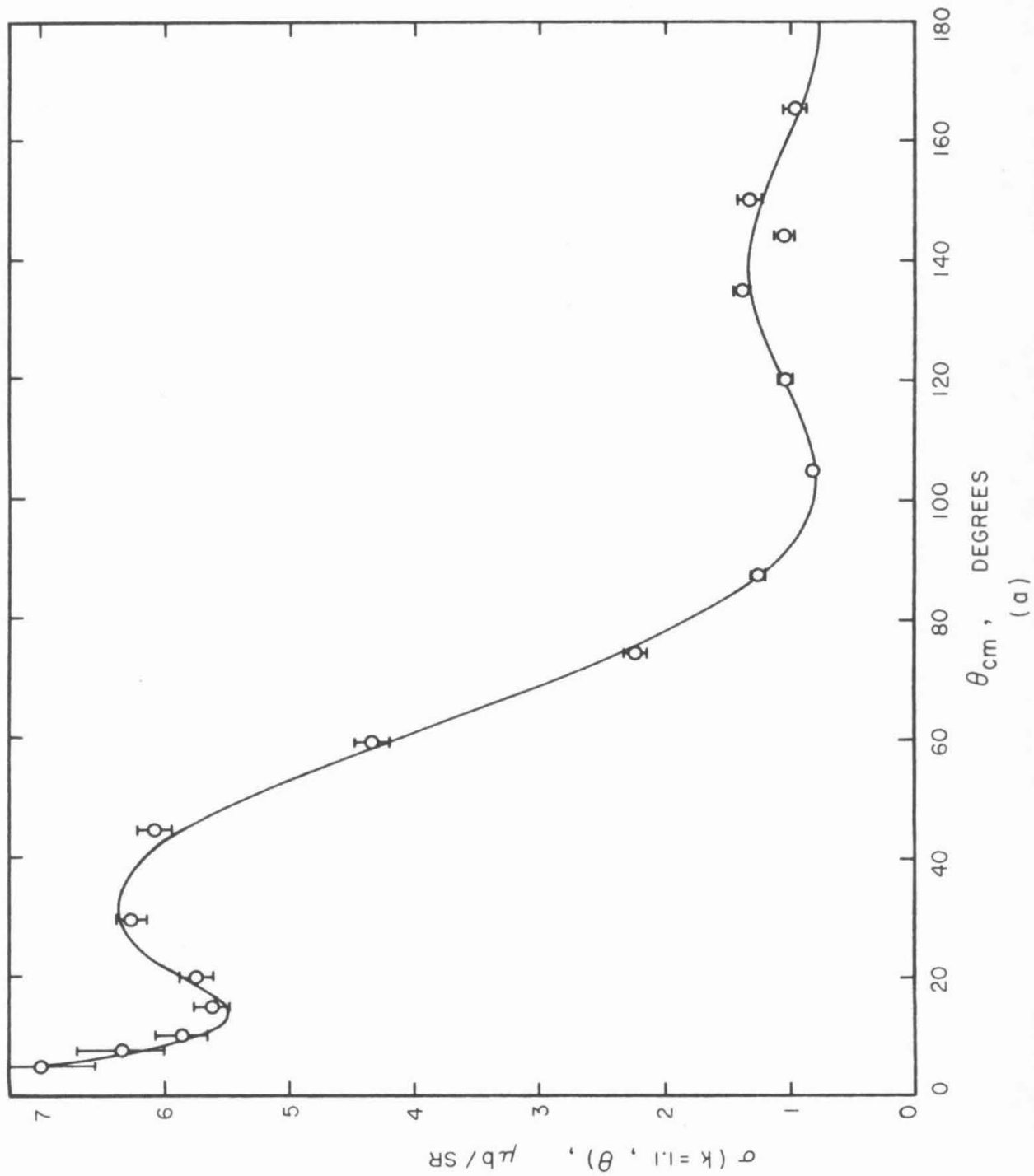
The solid curves are least squares fits of the Moravcsik type

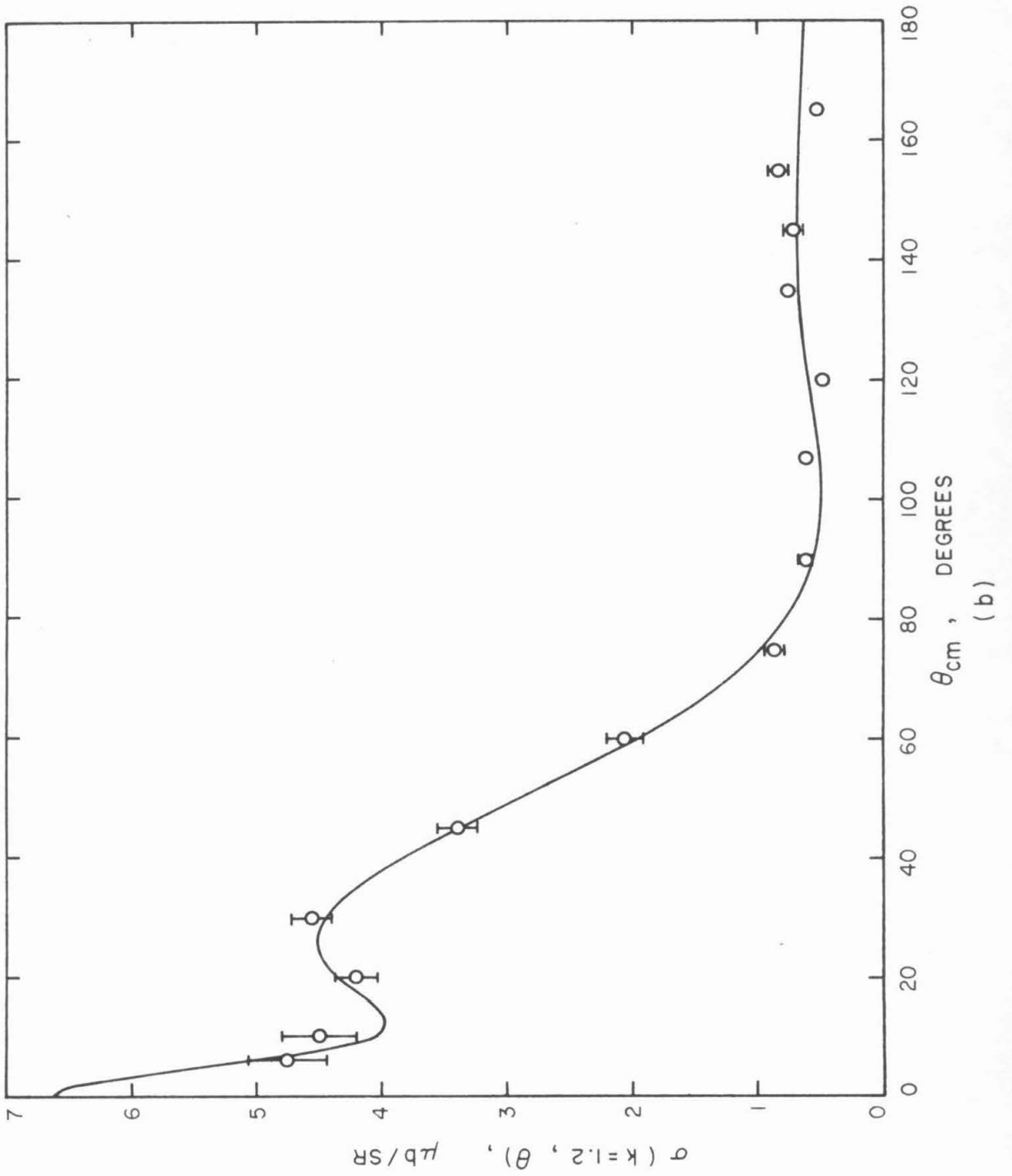
$$\sigma(\theta) = (1 - \beta \cos \theta)^{-2} \sum_{n=0}^N B_n \cos^n \theta$$

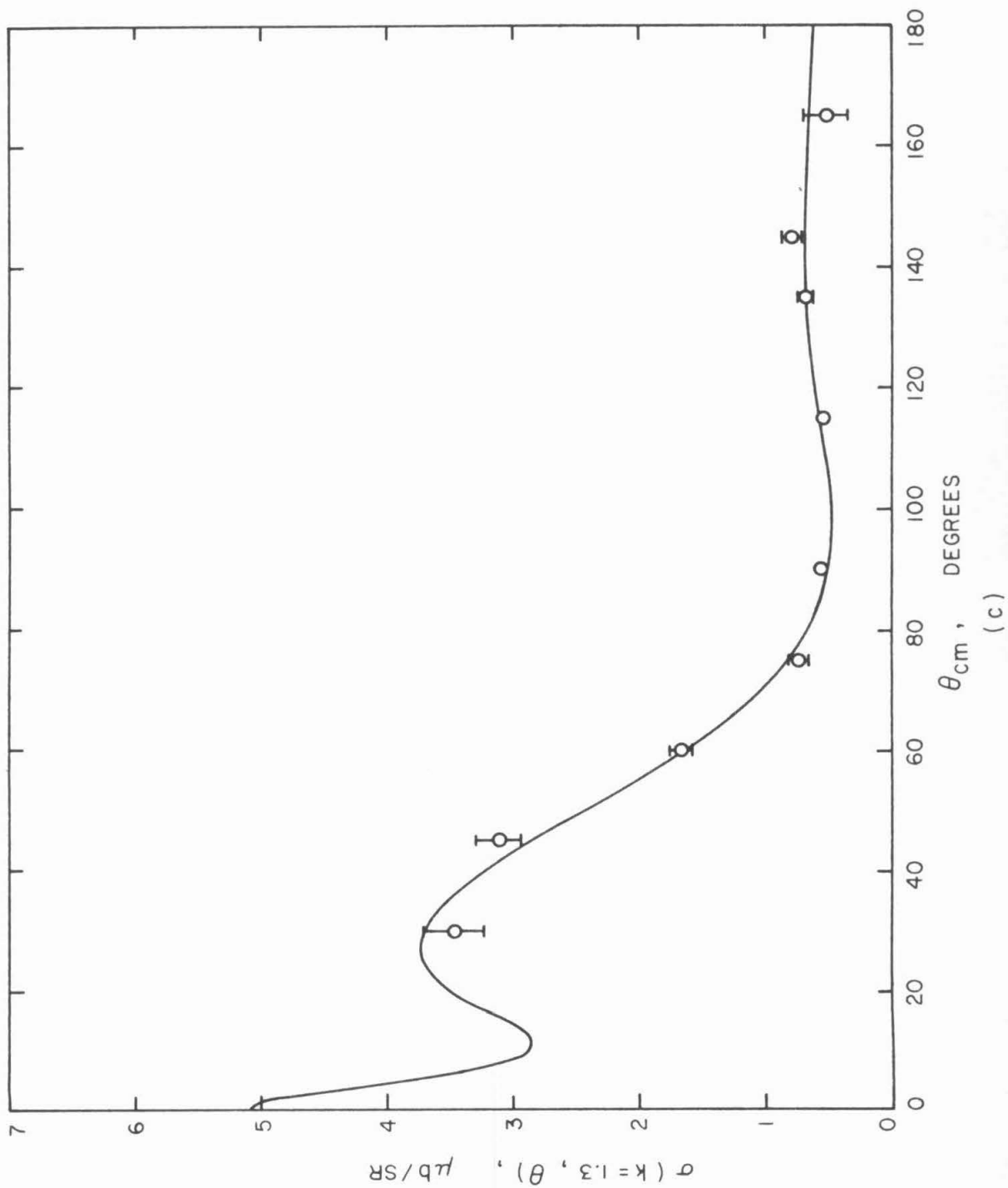
with $N = 6$.

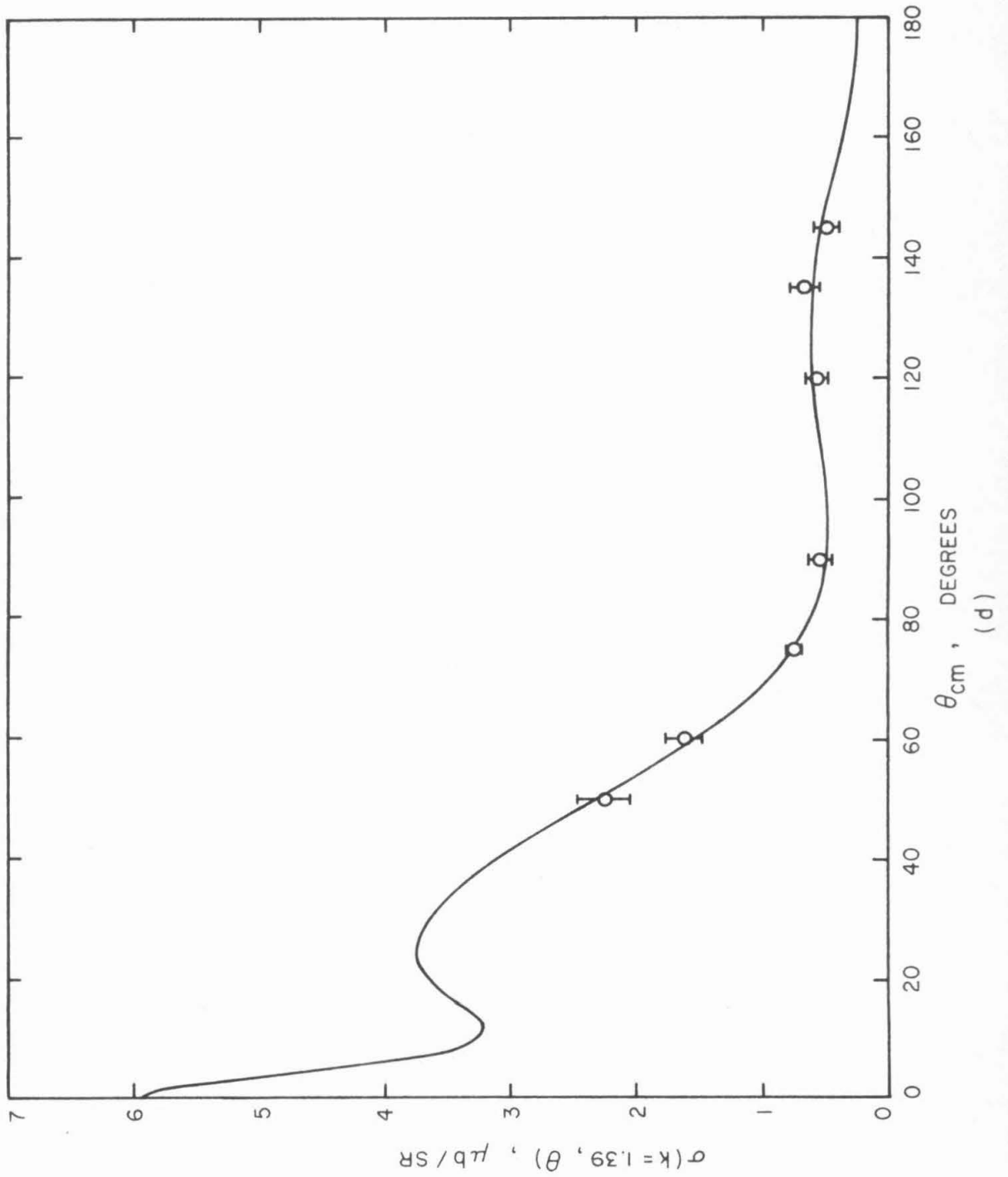
Polynomial fits are poor in comparison with those of the Moravcsik type.

Not shown are some artificial data points used in the fitting process to keep the fit "sensible" in a region of few data points. The pion nucleon coupling constant as it enters the formula for the residue at the pion pole was also used as input data in the fitting procedure. (See Table 5.) The errors shown are those of a statistical nature only.









VI. ANALYSIS

A. GENERAL

At energies much above the first resonance no satisfactory theory of pion photoproduction as yet exists. It is thus necessary to use a phenomenological analysis to extract what information one can from the data. Several methods that have been used previously (e.g. see Boyden (6) or Dixon (5)) will be discussed in this chapter. They are polynomial fitting, multipole fitting, extrapolation of the cross section to 0° and 180° , and integration to obtain the total cross section.

B. MORAVCSIK POLYNOMIAL FITTING AND THE COUPLING CONSTANT

A polynomial of the form

$$\sigma(\theta) = (1 - \beta \cos \theta)^{-2} \sum_{n=0}^N B_n \cos^n \theta$$

has been shown by Moravcsik (10) to be superior to a polynomial without the retardation denominator, $(1 - \beta \cos \theta)^{-2}$, when fitting charged pion photoproduction data. Here β and θ are the center of momentum velocity and angle of the pion, respectively. A computer program written and described by Boyden (6) was used to perform a least squares fit to the data for various orders, N . Table 4 contains the results of this fitting program, and the curves for $N = 6$ are plotted with the data in Figure 6. The values of the residue at the pion pole and some estimated points given in Table 5 were also used in the least squares fitting. When the residue at the pion pole was not used as a

TABLE 4

Least Squares Coefficients

The results of the least squares fits to the data are listed here. The data includes the residues at the poles and the estimated points given in Table 5. The fitting function is of the form

$$\sigma(\theta) = (1 - \beta \cos \theta)^{-2} \sum_{n=0}^N B_n \cos^n \theta$$

as suggested by Moravcsik (10).

In addition the number of degrees of freedom, D , the value of χ^2 , the probability, P , of larger χ^2 , and the total cross section, σ_T , are given. The square of the pion-nucleon coupling constant, f^2 , was calculated using an extrapolation of the fitting curve (obtained without including the residue at the pole) to the pion pole.

k = 1.1

N	5	6	7	8
B ₀	1.27±0.04	1.11±0.04	1.09±0.05	1.09±0.05
B ₁	-0.22±0.12	0.80±0.17	0.59±0.20	0.56±0.26
B ₂	1.25±0.26	2.27±0.29	3.17±0.54	3.09±0.67
B ₃	-4.53±0.17	-10.11±0.68	-9.70±0.71	-9.33±1.88
B ₄	-0.04±0.36	1.43±0.40	-1.65±1.61	-1.57±1.65
B ₅	2.28±0.20	7.91±0.70	8.93±0.87	8.04±4.28
B ₆		-3.39±0.40	-0.93±1.31	-0.61±1.99
B ₇			-1.49±0.75	-0.90±2.85
B ₈				-0.35±1.63
D	11	10	9	8
χ ²	93.91	22.70	18.80	18.75
P	<0.01	0.013	0.03	0.017
f ²	0.136±0.011	0.080±0.013	0.053±0.017	
σ _T	31.16±0.34	31.90±0.35	32.10±0.36	32.09±0.36

k = 1.2

N	5	6	7	8
B ₀	0.53±0.04	0.56±0.05	0.59±0.05	0.69±0.06
B ₁	-0.10±0.09	-0.31±0.16	-0.25±0.16	-1.01±0.25
B ₂	2.05±0.24	1.92±0.25	1.32±0.54	0.26±0.60
B ₃	-3.41±0.17	-2.42±0.66	-2.42±0.66	4.39±1.81
B ₄	-1.47±0.28	-1.83±0.37	0.05±1.53	0.03±1.53
B ₅	2.41±0.18	1.49±0.62	0.60±0.94	-15.05±3.98
B ₆		0.59±0.38	-0.83±1.19	6.04±2.07
B ₇			0.95±0.75	11.01±2.60
B ₈				-6.36±1.57
D	9	8	7	6
χ ²	34.48	32.08	30.47	14.10
P	<0.01	<0.01	<0.01	0.025
f ²	0.061±0.016	0.074±0.020	0.101±0.028	
σ _T	18.34±0.37	18.24±0.38	18.76±0.38	18.43±0.38

k = 1.3

N	5	6	7
B ₀	0.48±0.04	0.50±0.04	0.50±0.04
B ₁	-0.37±0.13	-0.49±0.17	-0.53±0.21
B ₂	2.12±0.29	1.97±0.33	2.12±0.56
B ₃	-2.82±0.23	-2.05±0.79	-1.93±0.86
B ₄	-1.61±0.46	-1.81±0.50	-2.44±1.92
B ₅	2.21±0.28	1.32±0.91	1.49±1.04
B ₆		0.56±0.55	1.13±1.78
B ₇			-0.35±1.01
D	6	5	4
χ ²	10.99	9.95	9.84
P	0.09	0.08	0.05
σ _T	15.58±0.44	15.65±0.44	15.67±0.45

k = 1.39

N	5	6	7
B ₀	0.49±0.06	0.50±0.08	0.50±0.08
B ₁	-0.59±0.25	-0.67±0.36	-0.70±0.51
B ₂	2.26±0.49	2.17±0.57	2.25±1.12
B ₃	-2.18±0.40	-1.68±1.74	-1.57±2.20
B ₄	-2.44±0.88	-2.57±0.98	-2.98±5.15
B ₅	2.47±0.51	1.87±2.11	1.93±2.26
B ₆		0.38±1.30	0.82±5.60
B ₇			-0.25±3.14
D	4	3	2
χ ²	1.56	1.48	1.47
P	0.81	0.69	0.48
σ _T	14.85±0.90	15.05±1.13	15.05±1.13

TABLE 5

Residues at the Pole and Estimated Points

A. Residues at the Pole. (Using $f^2 = 0.081 \pm 6.7\%$)

k (GeV)	$\cos\theta = 1/\beta$	$(1-\beta\cos\theta)^2 \sigma(\theta) \Big _{\cos\theta = 1/\beta}$ ($\mu\text{b/SR}$)
1.1	1.0276	.00998 \pm .00067
1.2	1.0246	.00752 \pm .00050
1.3	1.0222	.00581 \pm .00039
1.39	1.0201	.00457 \pm .00031

B. Estimated Points.

k (GeV)	θ (degrees)	$\sigma(\theta)$ ($\mu\text{b/SR}$)
1.3	10	3.35 \pm 0.8
1.3	20	3.2 \pm 0.5
1.39	10	3.35 \pm 1.5
1.39	30	3.5 \pm 0.8

data point, the differential cross section was extrapolated to the pole as was done by Boyden (6). The pion-nucleon coupling constant, f , is related to the extrapolated value at the pole (see equation 1.5 in reference 11). The value of its square (f^2) obtained from the extrapolation is given in Table 4.

The low χ^2 probability at $k = 1.1$ and 1.2 GeV can be attributed to the large "scatter" of the data points at backward angles. For $N \geq 6$ the qualitative agreement with the data is quite good, while for smaller N it is noticeably poorer. The need to go no higher than $N = 6$ is consistent with previous results, (5), (6). It should be pointed out, however, that this is less certain at $k = 1.3$ and 1.39 GeV due to the somewhat incomplete angular distributions at these energies. The weighted average of f^2 for $N = 6$ is 0.078 ± 0.011 . This agrees well with the value of 0.087 ± 0.017 measured by Boyden (6).

C. THE 0° AND 180° CROSS SECTIONS

The effect of the pion pole vanishes at 0° and 180° , making the analysis at these points simpler. Boyden (6) has carried out such an analysis for k up to 1.0 GeV without reaching any definite conclusions in the region of the third resonance. Cross sections taken from the $N = 6$ Moravcsik fits are used to extend the curves given by Boyden. This is shown in Figure 7. The data of Hand and Schaerf (12) have been added because of the interesting peak shown at the second resonance. The dashed region is very poorly known. The large statistical errors on the data around $k = 1.0$ GeV make it difficult to

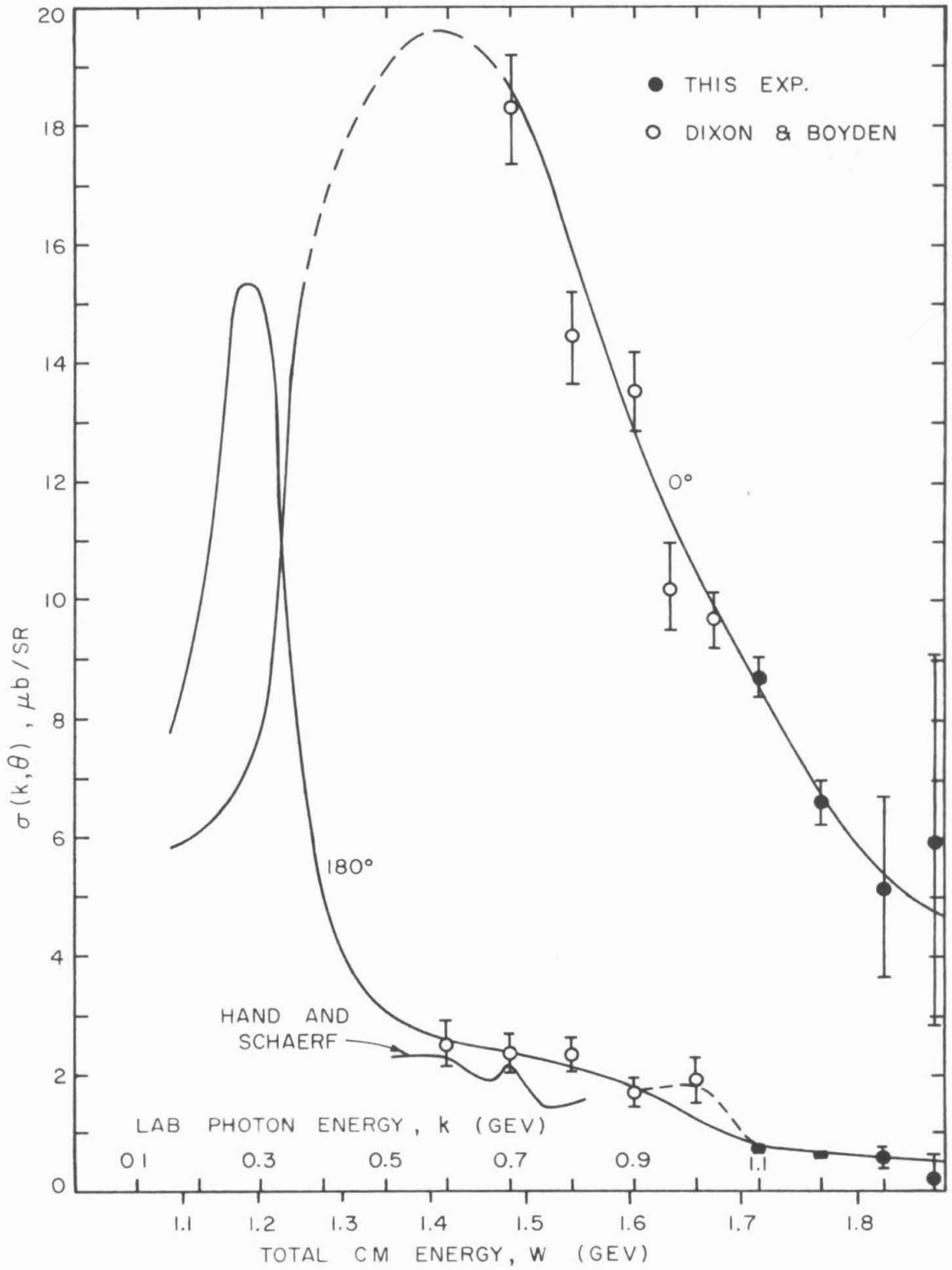


Figure 7. The 0° and 180° Cross Sections

see effects at the third resonance even a good deal larger than those seen by Hand and Schaerf at the second resonance. Thus it is still not possible to obtain any definite conclusions about the third resonance from this analysis; a multipole analysis must be attempted.

D. THE TOTAL CROSS SECTION

The total cross section, σ_T , is obtained by integrating the least squares fitting curves.

$$\sigma_T = 2\pi \int_0^\pi \sigma(\theta) \sin \theta \, d\theta$$

This is included in Table 4. The values from the sixth order curves are plotted in Figure 8, together with the results at lower energies (5), (6). The peak of the third resonance is seen to be very close to $k = 1.0$ GeV. The leveling-off of σ_T above $k = 1.3$ GeV may be an indication of the fourth resonance, which is observed in scattering experiments (3) at a total c. m. energy of 1.922 GeV.

E. MULTIPOLE ANALYSIS

An attempt was made to perform a multipole analysis using all of the pion photoproduction data currently available. A high speed computer (the IBM 7090) was utilized in the calculation. The details of the fitting program are described elsewhere (13). The specific types of data used in this analysis were angular distributions of π^+ , π^0 , and the ratio of π^- to π^+ photoproduction, and the polarization of the recoil proton in π^0 photoproduction at 90° . The Born approximations for the s-channel, t-channel (pion pole), and u-channel (nucleon pole)

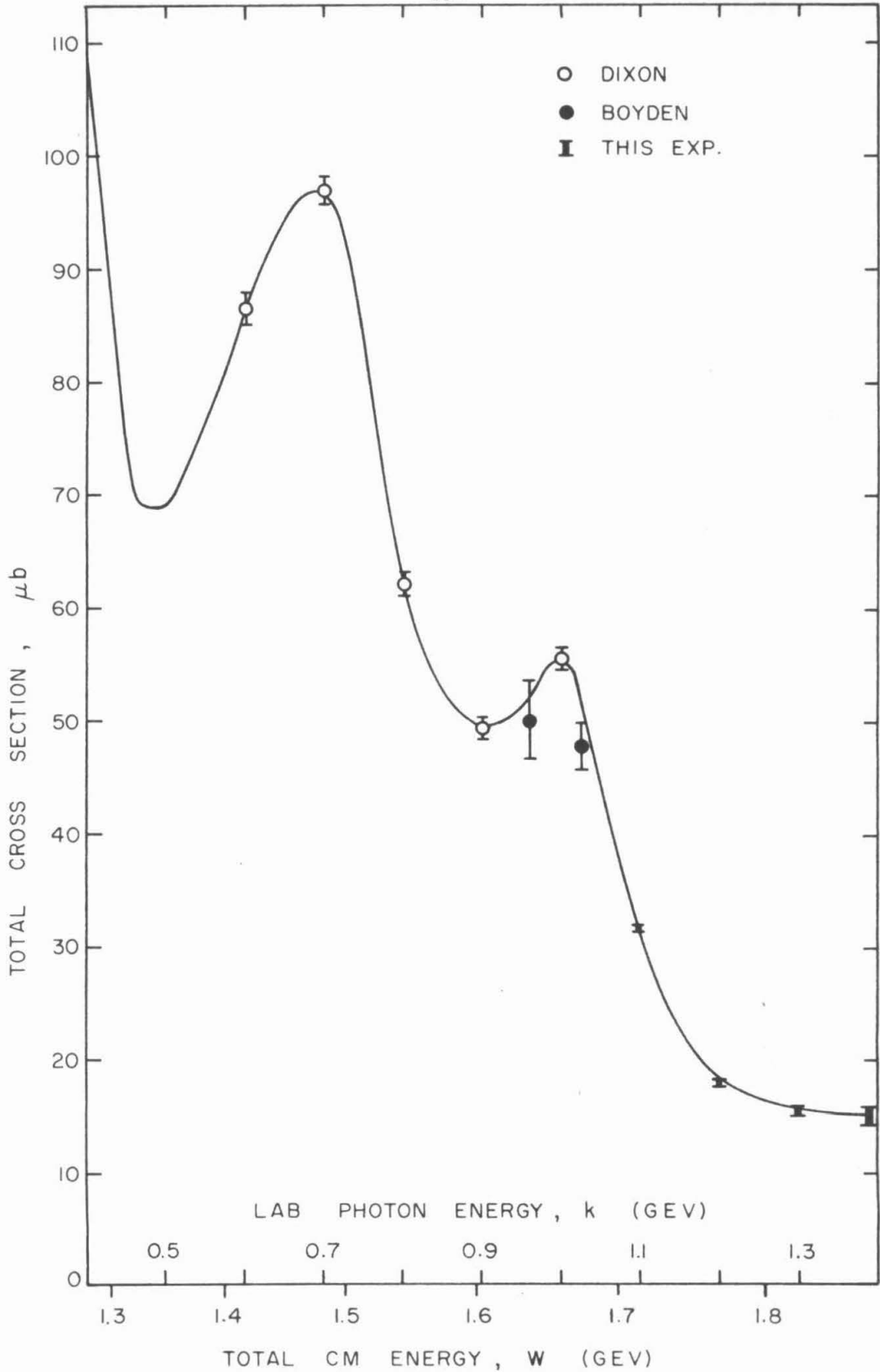


Figure 8. The Total Cross Section

diagrams were employed using both the charge and anomalous magnetic moment couplings. Although it was possible to perform this analysis in the region of the first resonance, great difficulties were encountered at higher energies. They were mainly due to the large size of the cross section produced by the nucleon pole at backward angles (e.g. see G. Höhler et al (14)). It was predominantly the magnetic moment coupling portion of the nucleon pole amplitude that was large. There is an indication that the use of Regge poles in this analysis may improve the situation, but no definite results have yet been obtained. The effort will be continued.

VII. CONCLUSIONS AND SUGGESTIONS

This experiment has shown the third resonance peak in π^+ photoproduction to lie very close to $k = 1.0$ GeV. The leveling off of the total cross section at the highest energies investigated here may be due to the fourth pion-nucleon resonance. The general shape of the angular distributions changes remarkably little from $k = 1.0$ to 1.39 GeV. However, the angular distributions at $k = 1.3$ and 1.39 GeV reported here are incomplete (mainly in the forward direction) making it difficult to draw any conclusions about the fourth resonance. Extension of this experiment to higher energies might provide information of value in identifying the fourth resonance.

It would be very useful to have a theory of pion photoproduction at high energies. Since this seems hard to come by, data on other types of reactions at these energies would at least aid in the phenomenological analysis. Useful measurements would include those of the angular distributions of π^0 and π^- (from the π^- to π^+ ratio) and the polarizations of the recoil nucleons in π^0 and π^+ photoproduction.

The square of the pion-nucleon coupling constant, f^2 , has been found to be 0.078 ± 0.011 from extrapolations of the sixth order Moravcsik fitting curves. The results obtained from the present data are rather sensitive to the fitting order chosen. However, an experiment might be designed which could circumvent the problems caused by the very large number of electrons near 0° . A more accurate determination of the pion-nucleon coupling constant should then be possible.

The application of the concepts of Regge poles to the analysis of

pion photoproduction is a most promising lead and should certainly be investigated. Replacing the Born approximations by Regge pole amplitudes will tend to reduce the cross sections, which is exactly what the multipole analysis attempted here has indicated is necessary. It would be most interesting to investigate whether or not the Regge poles can have an appreciable effect at "medium" energies such as those involved in this experiment.

APPENDIX I

COUNTER EFFICIENCIES

The calculation of the pion flux from the counting rates is based on the knowledge of the efficiencies of several counter systems. The efficiency of each counter system in detecting various particles was measured independently using well known methods.

Figure A1 gives the efficiencies which vary with momentum. The difficulty of selecting a really pure beam of pions at the high momenta made it necessary to measure $\eta_{\chi\pi}$ at lower momenta and extend it to the range used, where it is not expected to decrease. The electrons used in measuring η_{Ee} were photoproduced in a 0.02 inch lead target. To prevent flooding of the counters the photon beam had been greatly reduced in intensity by passing it through two to three inches of lead placed ahead of the sweeping magnet. The curves for η_{Ee} have been corrected for a background contamination amounting to 0.0018 ± 0.0014 for the double converter and 0.0033 ± 0.0013 for the single converter. This contamination consisted of electrons produced in the air, probably in or after the spectrometer magnet, which was at zero degrees. These electrons would have momenta lower than those produced in the target.

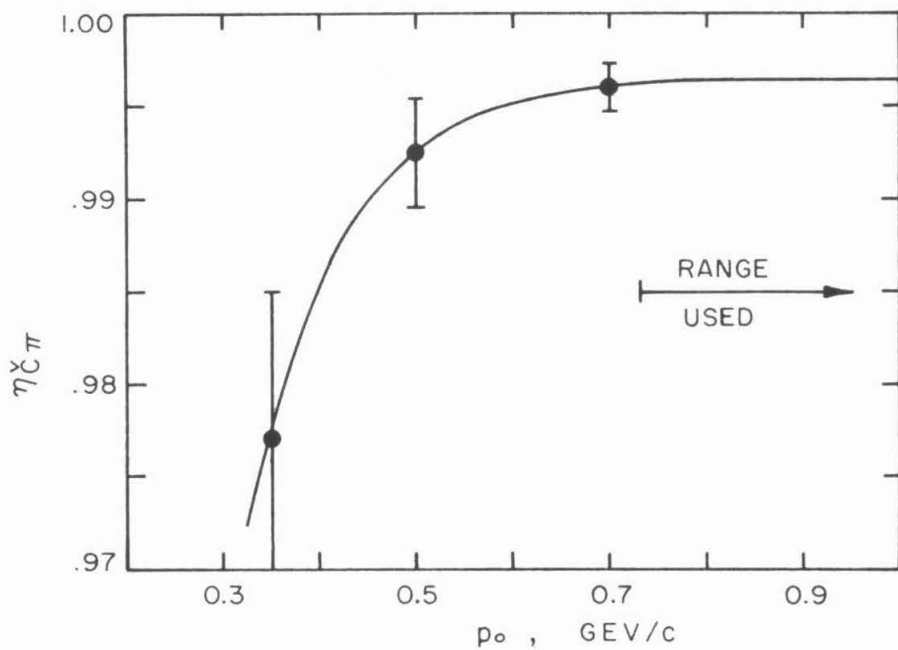
The fan counter efficiencies were measured by placing a specially built long, narrow counter behind each of the back fan counters in turn. The average efficiency was $\eta_{FANS\pi} = 0.970 \pm .003$.

In measuring the efficiency of the time of flight system (A1 to C2) a lead wall was built around A1 to prevent particles not passing through

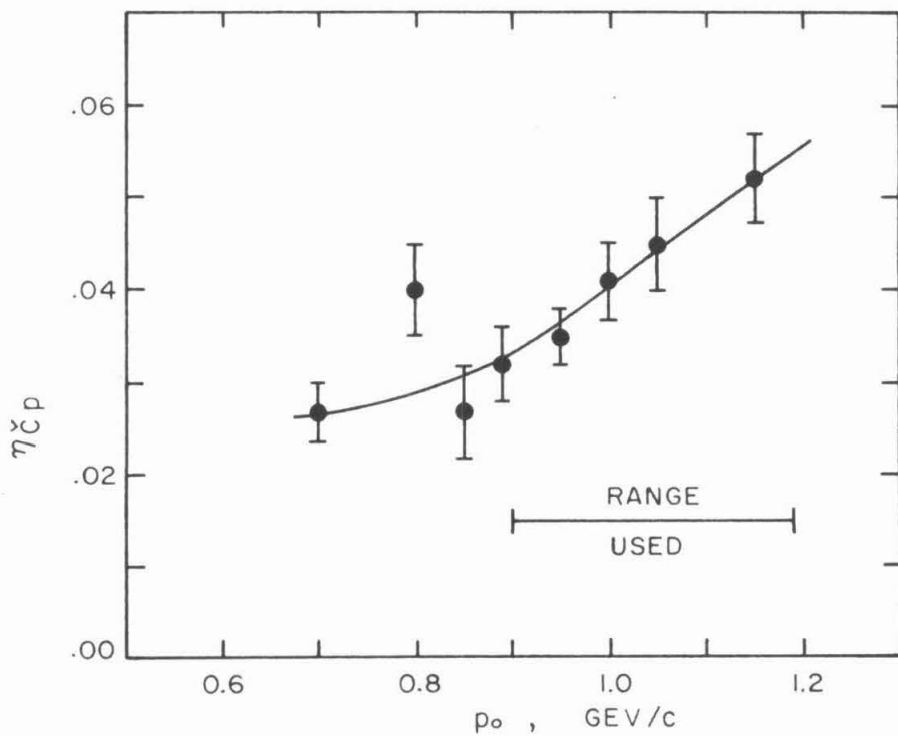
Figure A1. Cherenkov Counter and Electron Detector
Efficiencies vs Spectrometer Central Momentum

(a)	$\eta_{C\pi}^Y$	(value used: $0.9960 \pm .0012$)
		Errors
(b)	η_{Cp}^Y	$\pm .002$
(c)	η_{Ee}	$\pm .002$
(d)	$\eta_{E\pi}$	$\pm .005$
(e)	η_{Ep}	$\pm .005$

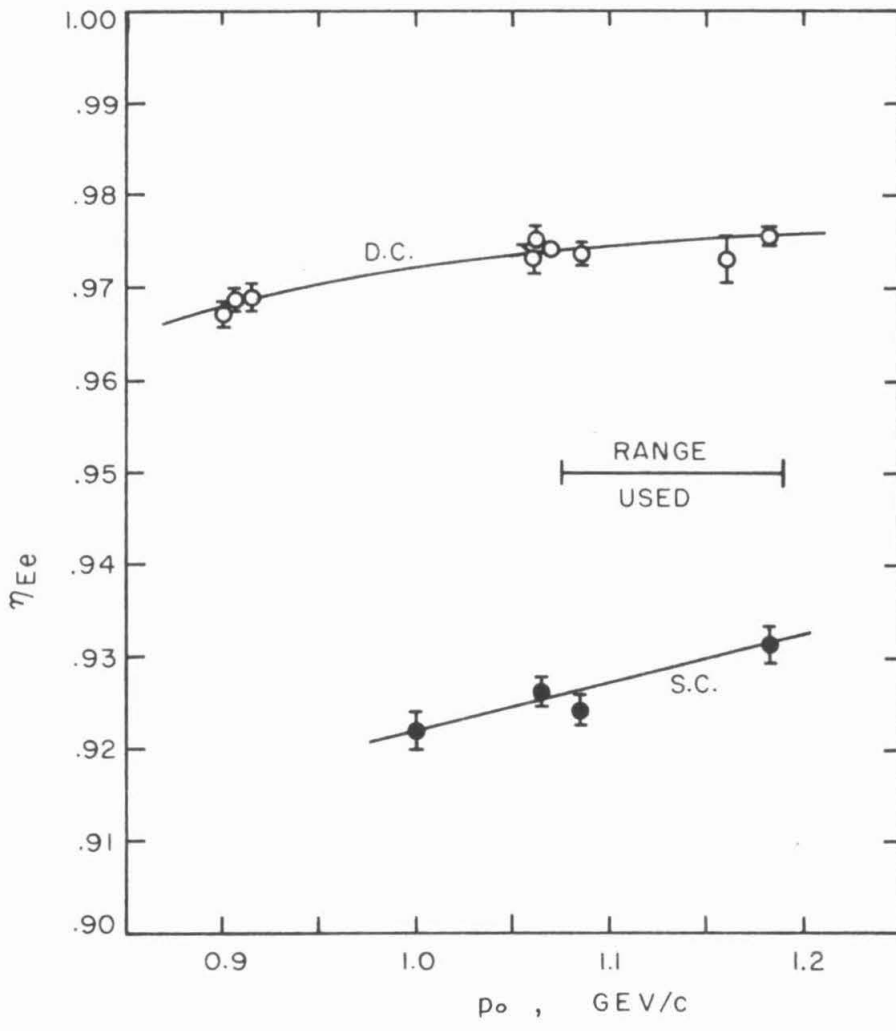
The ranges in which these efficiencies are used in the data reduction are shown in each Figure. For the electron detector, S.C. and D.C. indicate single converter and double converter systems respectively.



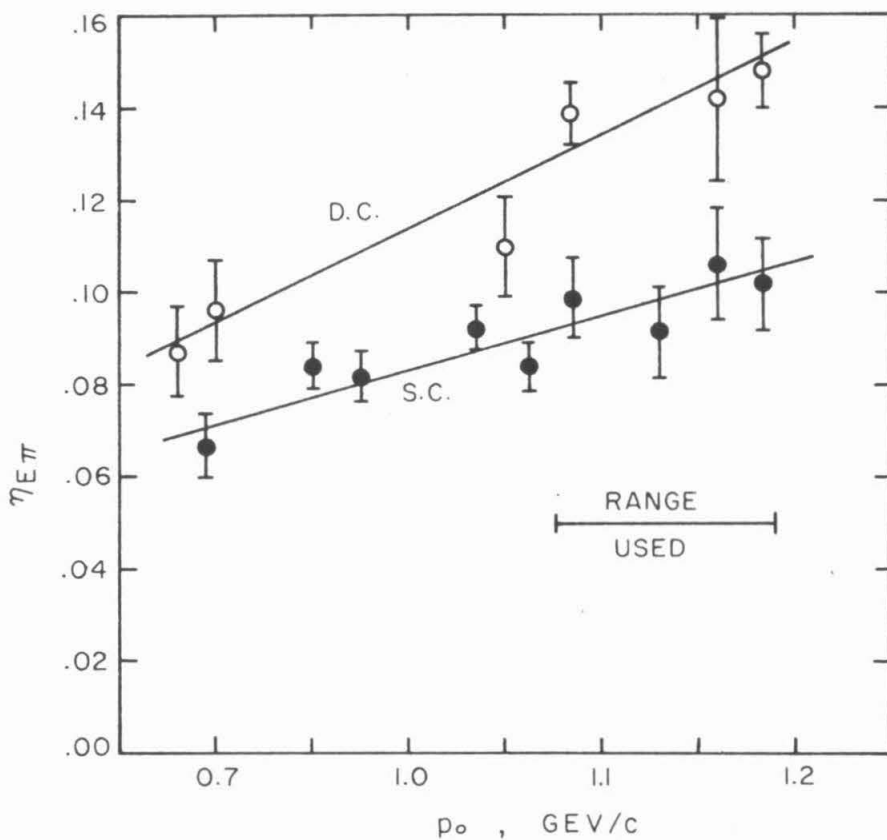
(a)



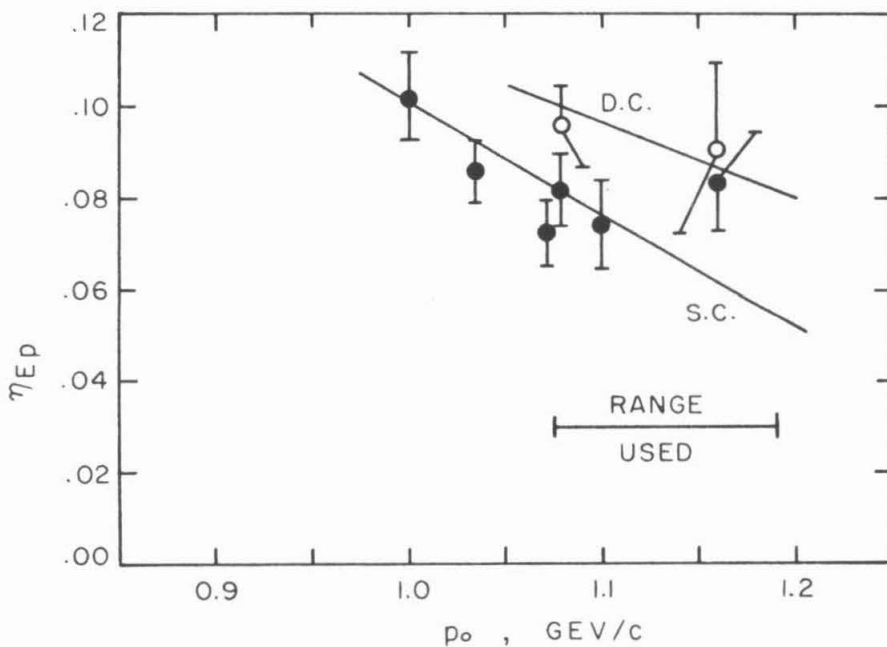
(b)



(c)



(d)



(e)

Al from being counted. At a momentum of 0.45 GeV/c, where all protons stop in the lead absorber in front of C3, the value $\eta_{T\pi} = 0.9964 \pm .0014$ was obtained.

The efficiency of one counter, C1, was found to be $0.993 \pm .002$. However, the nine out of 1289 particles that did not give a count above the bias gave no count at all, and it is assumed that these missed C1 completely. Therefore the efficiency of a single dE/dx counter is taken to be 100%.

The procedure used by Boyden (6) to insure that the various efficiencies would be stable throughout the course of the experiment was also followed here. Using the large number of electrons found at zero degrees (this is the same set up used for measuring η_{Ee}) with the absorbers removed to eliminate electron showers and thus large pulses, each bias in turn was set to a preselected value and the corresponding amplifier gain was adjusted to give an efficiency of 50% for each counter. All biases were returned to their normal operating values after this calibration. During the approximately eight months of data taking, no noticeable drift in the efficiencies could be detected.

APPENDIX II
NUCLEAR ABSORPTION

The same method that was used by Boyden (6) for measuring the absorption of pions by material within the counter box was followed here. The results were in very good agreement with those of Boyden and the statistical errors have been reduced appreciably. Absorbers were placed between C2 and C3 and the number not giving counts in C3 were considered to be absorbed. The counting rate with no absorber in place was subtracted to obtain the net absorption from the absorber being measured. The results were:

Absorber	Fraction Absorbed	Momentum, p_0 (GeV)
1/2" Lead	0.027 \pm .004	0.52
	0.029 \pm .007	0.90
	0.028 \pm .004	average
1" Lead	0.073 \pm .012	0.9
1 1/2" Lucite	0.025 \pm .005	0.52

It was assumed that the material of C2 and lucite have similar absorptive properties. The absorption of lucite was measured with the 1/2" Pb absorber in place to prevent any low energy secondaries from counting. This 1/2" absorber was always in front of C3 during the course of the experiment. Boyden previously found the absorption to be independent of the pion momentum; this is verified by the results given above.

For material other than the lead absorbers and C2 the geometrical absorption length was used. Dixon (5) has shown this is roughly consistent with measured values for material in front of the counter box. Accurate direct measurement of the absorption in material in front of C2 would have been prohibitively time consuming. The calculated values of the fractional geometrical absorption length for all material in front of C2 are:

H.E. 0.102

M.E. 0.054

The absorption corrections, A_{π} , for the various configurations are:

H.E. S.C. 0.861 \pm 0.005

H.E. D.C. 0.820 \pm 0.013

M.E. 0.907 \pm 0.005

The errors listed are those from the measured absorptions only.

The points at $k = 1.3$, $\theta = 30^{\circ}$ and $k = 1.39$, $\theta = 50^{\circ}$ were measured with a one inch thick piece of lead in front of the magnet to reduce the pion momentum to a value which the magnet could accept. (The momentum was reduced by about 40 MeV/c). The reduction of pion flux in this lead was assumed to be the same as that at a slightly lower momentum. The absorption at the latter momentum was measured directly. (It was necessary to change the magnetic field and to correct for the change in $\Delta p/p_0$.) It was found that 0.76 ± 0.03 of the incident pions were counted after passing through the lead. This fraction appears as part of A_{π} in the table of results in chapter V.

APPENDIX III

DECAY AND SCATTERING CORRECTIONS

Typically ten to twenty per cent of the pions decay while traveling from the hydrogen target to the counter telescope via the reaction $\pi^+ \rightarrow \mu^+ + \nu$ which has a mean lifetime of $(2.56 \pm .05) \times 10^{-8}$ seconds in the rest system of the pion. Some of the muons will give counts indistinguishable from those produced by the pions. This number can be calculated from the kinematics of the pion decay, and the geometry of the magnetic spectrometer and counter system. About the only practical way to carry out such a calculation is to use a Monte Carlo technique on a very fast computer. A procedure somewhat similar to that used by Boyden (6) is employed. The present results agree very well with his in regions where they are comparable.

A computer program was written to simulate the magnetic spectrometer and counter system. "Pions" were then sent through the system with initial position in the target and initial angles picked randomly. Typically a series of about twenty evenly spaced values of the pion momentum was used at each spectrometer setting, with several hundred "pions" used at each momentum. The computer counted all "pions" successfully reaching C2. Each "pion" was then restarted with the same initial values and allowed to decay at a preselected distance and counted as a "muon" if it reached C2. The decay distances formed a series of about fifteen evenly spaced values along the 660 cm flight path in the high energy configuration or the 416 cm flight path in the medium energy configuration. Figure A2 shows schematically the magnetic

spectrometer and counter system with the input parameters as they appear in the computer program. Table A1 gives the values of all input parameters to the decay correction program.

Let the effective solid angle (in SR) of the spectrometer be defined as 4π times the fraction of particles (all of the same momentum and isotropically emitted from the target) which would pass properly through the counter system. The effective solid angles for pions and muons are obtained from the program and are plotted as functions of momentum in Figures A3 and A4 respectively. (Table A3 in Appendix IV gives a comparison of the calculated magnet acceptance, $\Delta\Omega \Delta p/p_0$, with measured values.) The quotient of the integral (over the obtainable pion momenta) of the muon momentum response function by the integral of the pion momentum response function is the fraction of muons which will give counts in the system. It should be noted that errors in the magnet simulation will tend to cancel when this division is made. Because of the large amount of computer time involved only the points shown in Figure A4 were calculated, the others being obtained by interpolation. The decay correction, which consists of the fraction of pions decaying in the system times one minus the fraction of muons counted, is given in Table 3 in chapter V.

The same magnet simulation computer program that was used for the decay correction calculations was modified to investigate the multiple scattering of pions along their flight path. The Monte Carlo technique was again used and the number of "pion" counts lost or gained due to multiple scattering was tallied by the computer. In order to simplify the calculation, the air along the flight path was lumped into five planes. Table A2

Figure A2. Decay Correction Coordinate
System and Parameters

The magnetic spectrometer is shown schematically in the top and side views. Each parameter which contains an X or a Y refers respectively to an x- or y-coordinate of the designated point. Angles are considered positive in the sense indicated. The values of the parameters are given in Table A1.

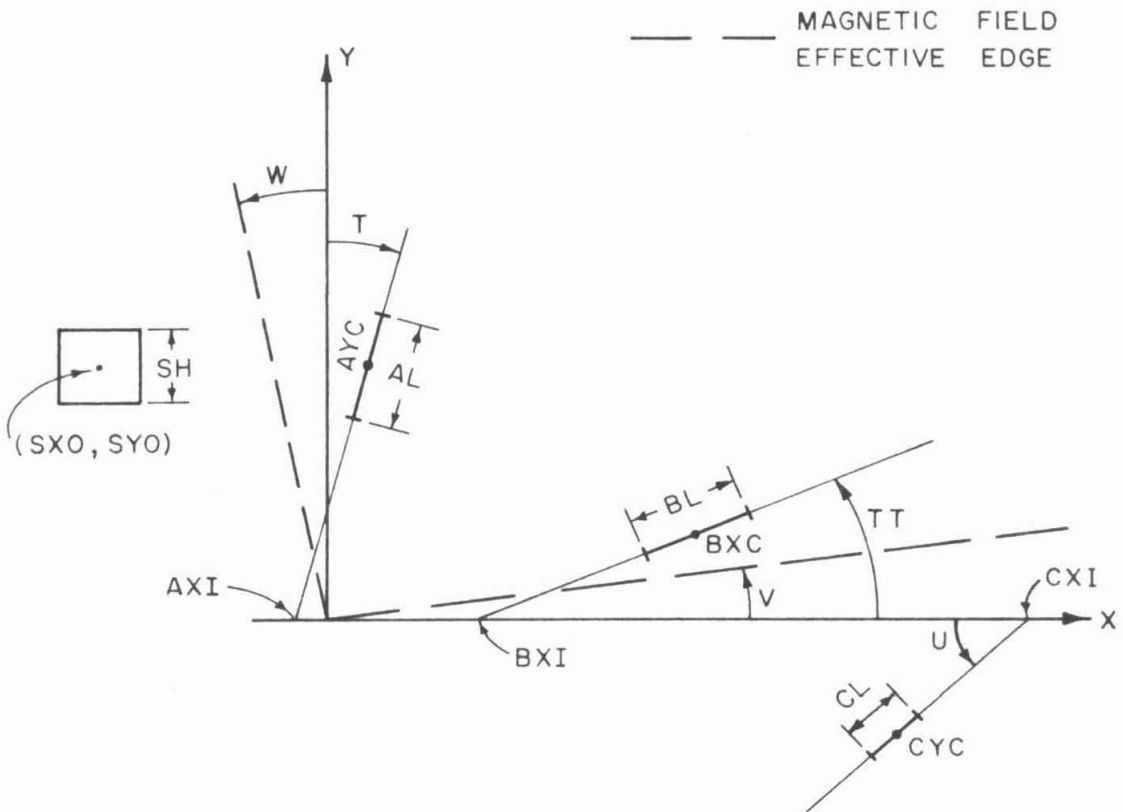
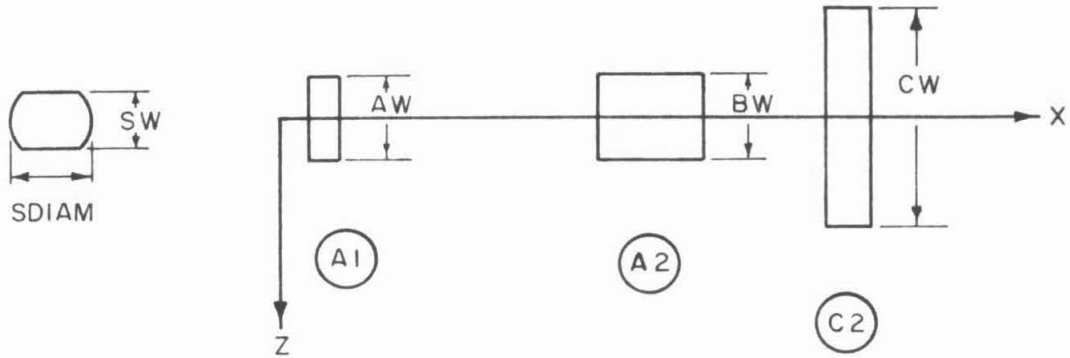


TABLE A1

Parameters for the Decay Correction Program

RHOC = radius of curvature of the trajectories in the magnetic field.

FFF (and FFR) are the fringe field correction parameters. The angular deflection upon entering (or leaving) the magnetic field, measured in the plane normal to the x-y plane and containing the trajectory is given by

$$\theta_z = (FFF) z \tan \theta'$$

where θ' is the angle between the pion path and the perpendicular to the field edge.

S is the beam shape parameter. The beam intensity distribution is approximated by $e^{-r^2/S}$ where r is the distance from the beam center in centimeters.

All other parameters are shown in Figure A2. The lengths are given in centimeters and the angles in radians.

TABLE A1
DECAY CORRECTION PARAMETERS

	H.E. A1	H.E. A1 C2S	H.E. A2L	H.E. A2S	M.E. A1 C2S
SXD	-295.4	-295.4	-295.4	-295.4	-145.1
SYD	59.51	59.51	59.51	59.51	54.35
SDIAM	7.60	7.60	7.60	7.60	7.60
SW	4.1	4.1	4.1	4.1	4.1
SH	4.9	4.9	4.9	4.9	4.9
S	3.8	3.8	3.8	3.8	3.8
RHUC	266.7	266.7	266.7	266.7	139.4
AL	31.34	31.34	66.0	66.0	31.34
AW	8.23	8.23	7.62	7.62	8.23
AYC	59.36	59.36	56.33	56.33	54.02
AXI	-23.0	-23.0	13.5	13.5	5.6
BL	99.0	99.0	30.07	15.24	99.0
BW	7.62	7.62	7.59	7.59	7.62
BXC	69.0	69.0	93.44	93.44	89.0
BXI	-13.5	-13.5	0.0	0.0	-40.6
CL	12.06	5.08	12.06	12.06	5.08
CW	27.94	27.94	27.94	27.94	27.94
CYC	-92.41	-92.41	-92.41	-92.41	-111.51
CXI	378.13	378.13	378.13	378.13	334.87
FFF	.0037	.0037	.0037	.0037	.0037
FFR	.0037	.0037	.0037	.0037	.0037
T	.05236	.05236	.0	.0	.07854
TT	.4800	.4800	.309214	.309214	.152
U	1.094612	1.094612	1.094612	1.094612	.695514
V	.309214	.309214	.309214	.309214	.040434
W	.450877	.450877	.450877	.450877	.030252

Figure A3. Magnetic Spectrometer Momentum Response

The abscissa is the fractional difference of the pion momentum from the central momentum, p_0 . ($\Delta p = p - p_0$)

(a) High Energy Magnet using the front aperture defining counter, A1.

(A) This curve was obtained from the Magnet Report (9) by a rough interpolation between the curves for a point source and a 3" H_2 target.

All the following curves were obtained from the Monte Carlo decay correction calculation.

(B) Standard momentum defining counter, C2L.

(C) Small momentum defining counter, C2S, (approximately half the size of C2L).

(b) High Energy Magnet using the rear aperture counter, A2, and Standard C2.

(D) Large A2.

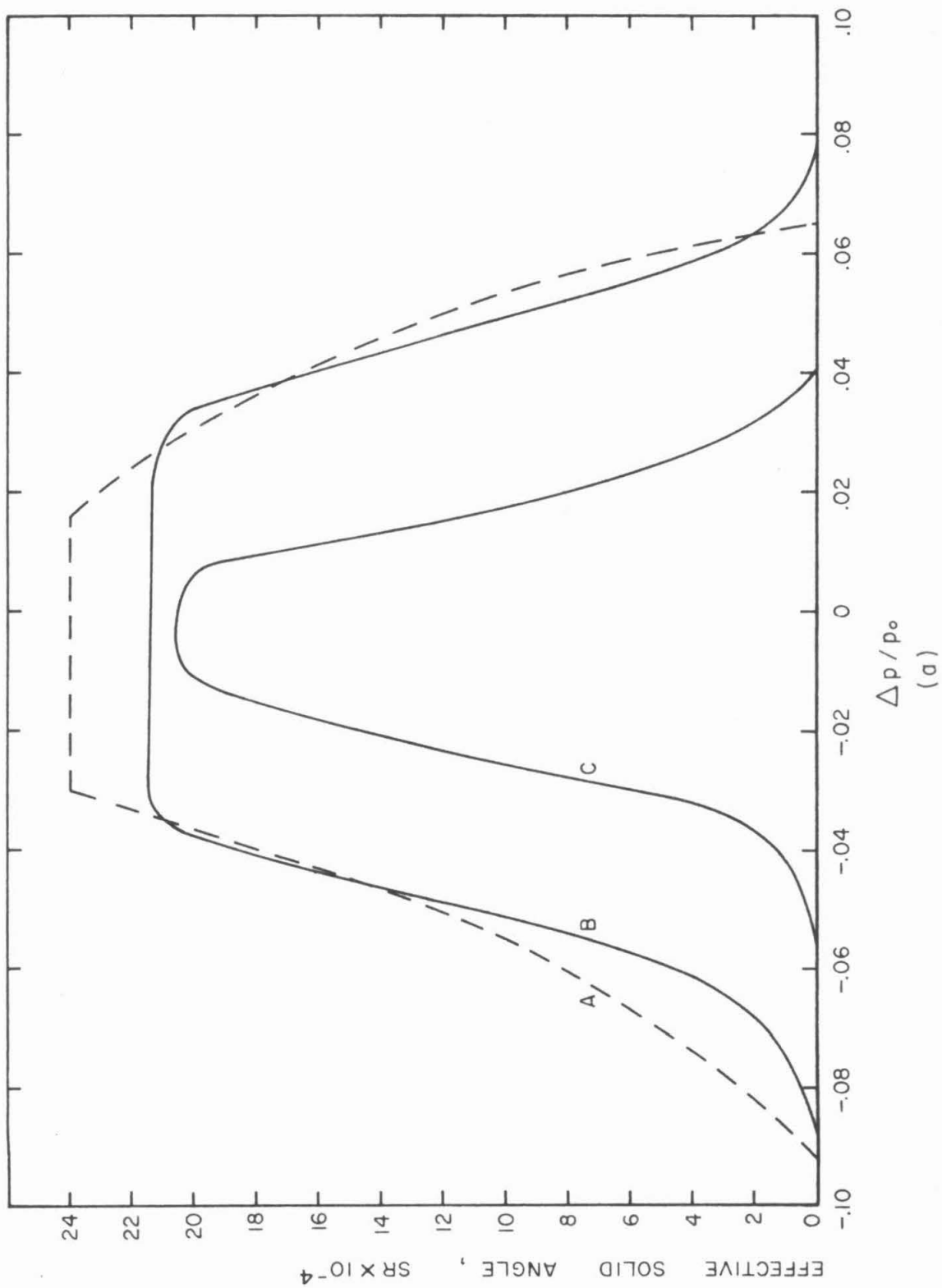
(E) Small A2.

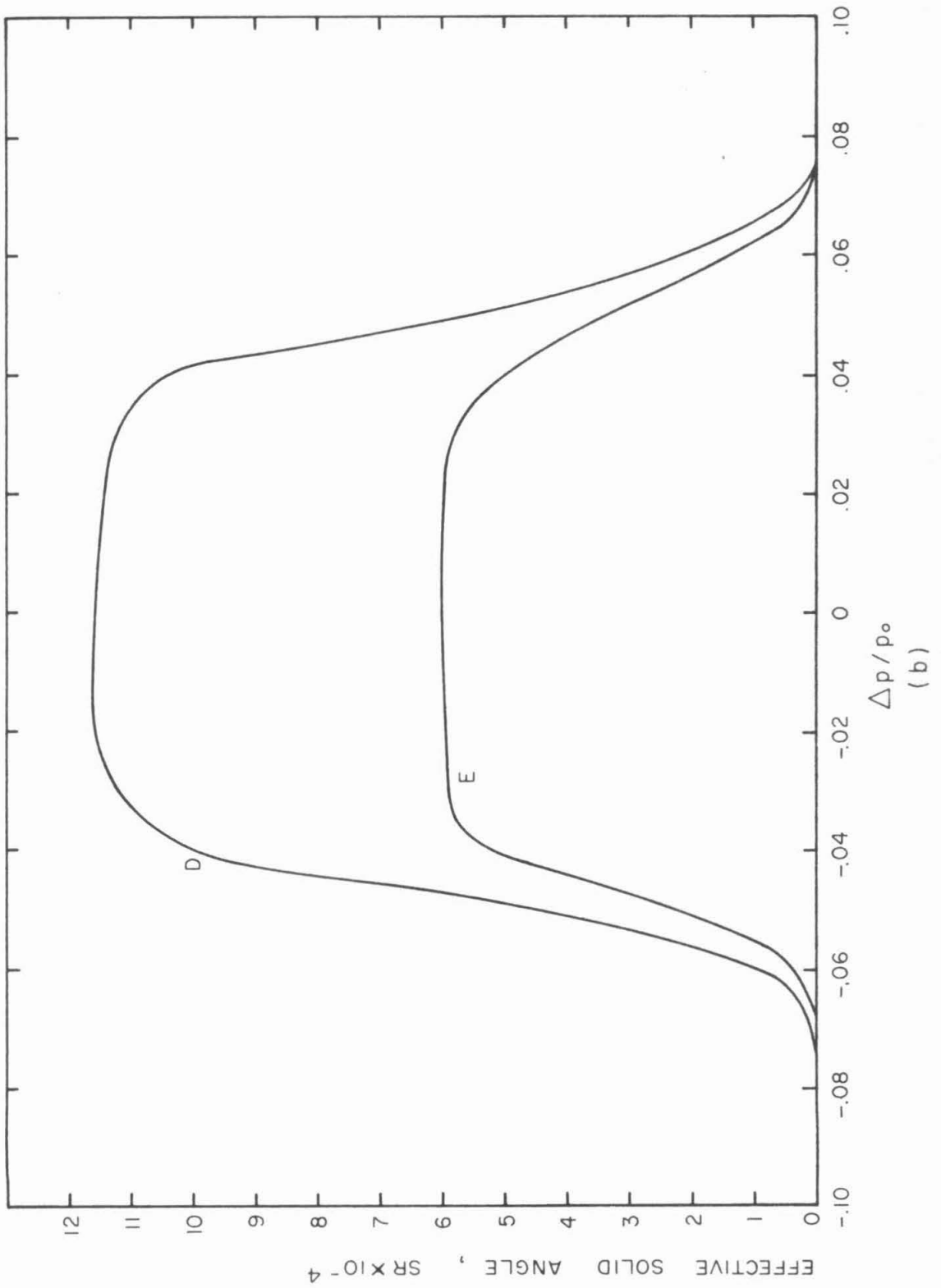
(c) Medium Energy Magnet using A1 and small C2 (curve F).

The numbers of points calculated to obtain these curves are as follows:

B, 106 points; C, 31 points; D, 33 points; E, 31 points; F, 55 points.

The errors on these points, which result from the statistical errors on the number of "successes" counted, are typically between 5 and 10% at the peak of the curve and decrease in absolute size as the square root of the value along the curve.





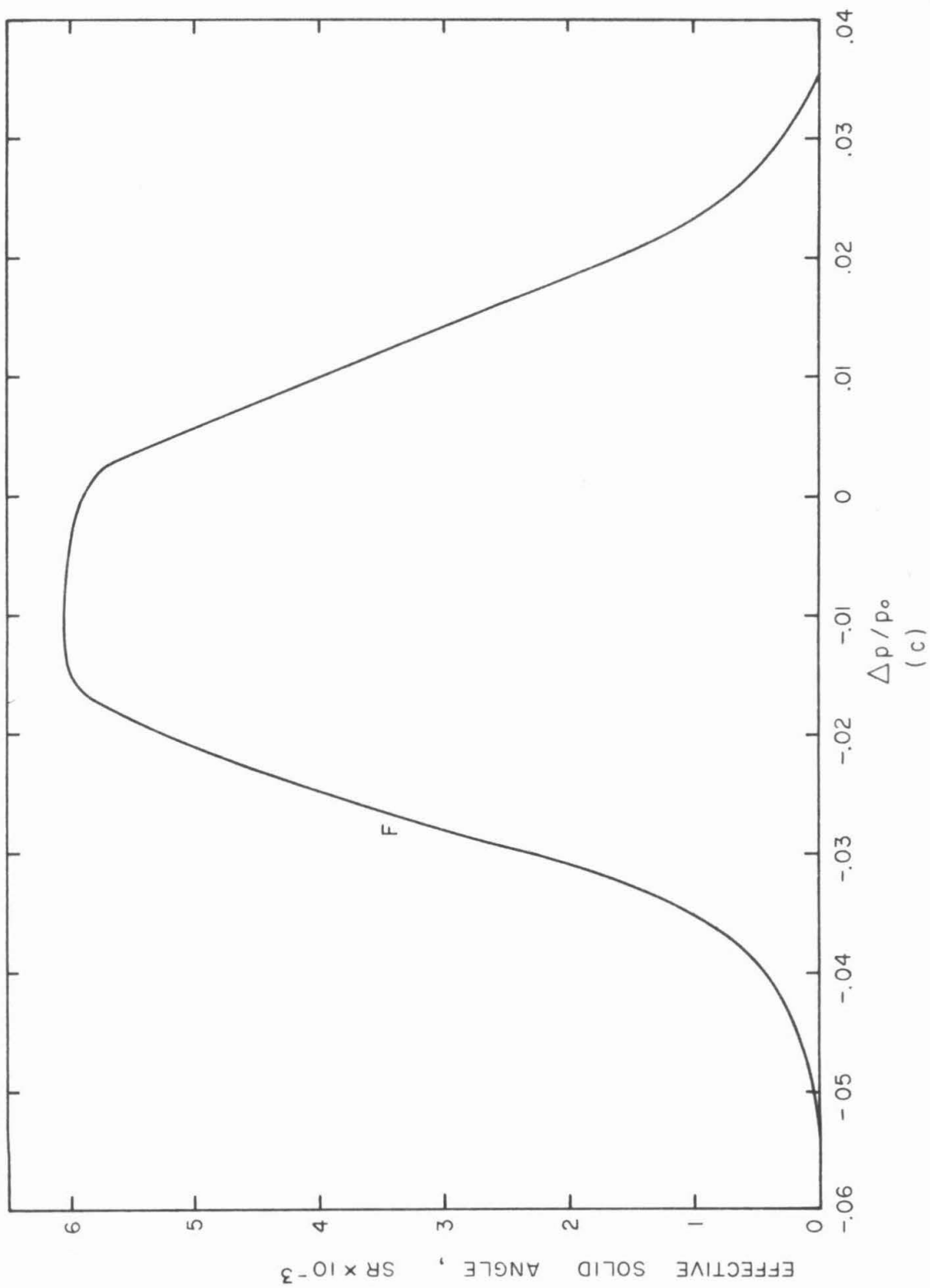
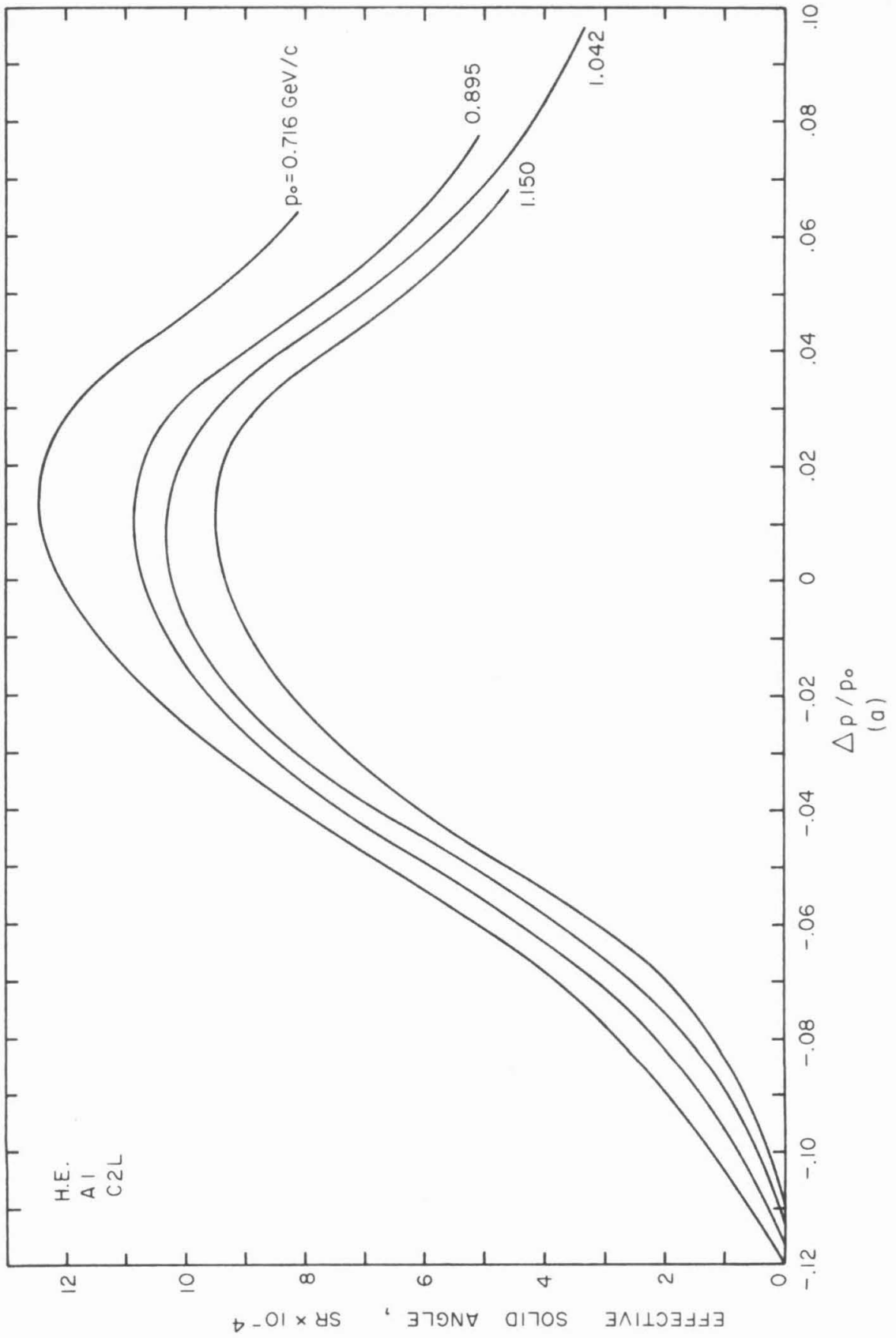


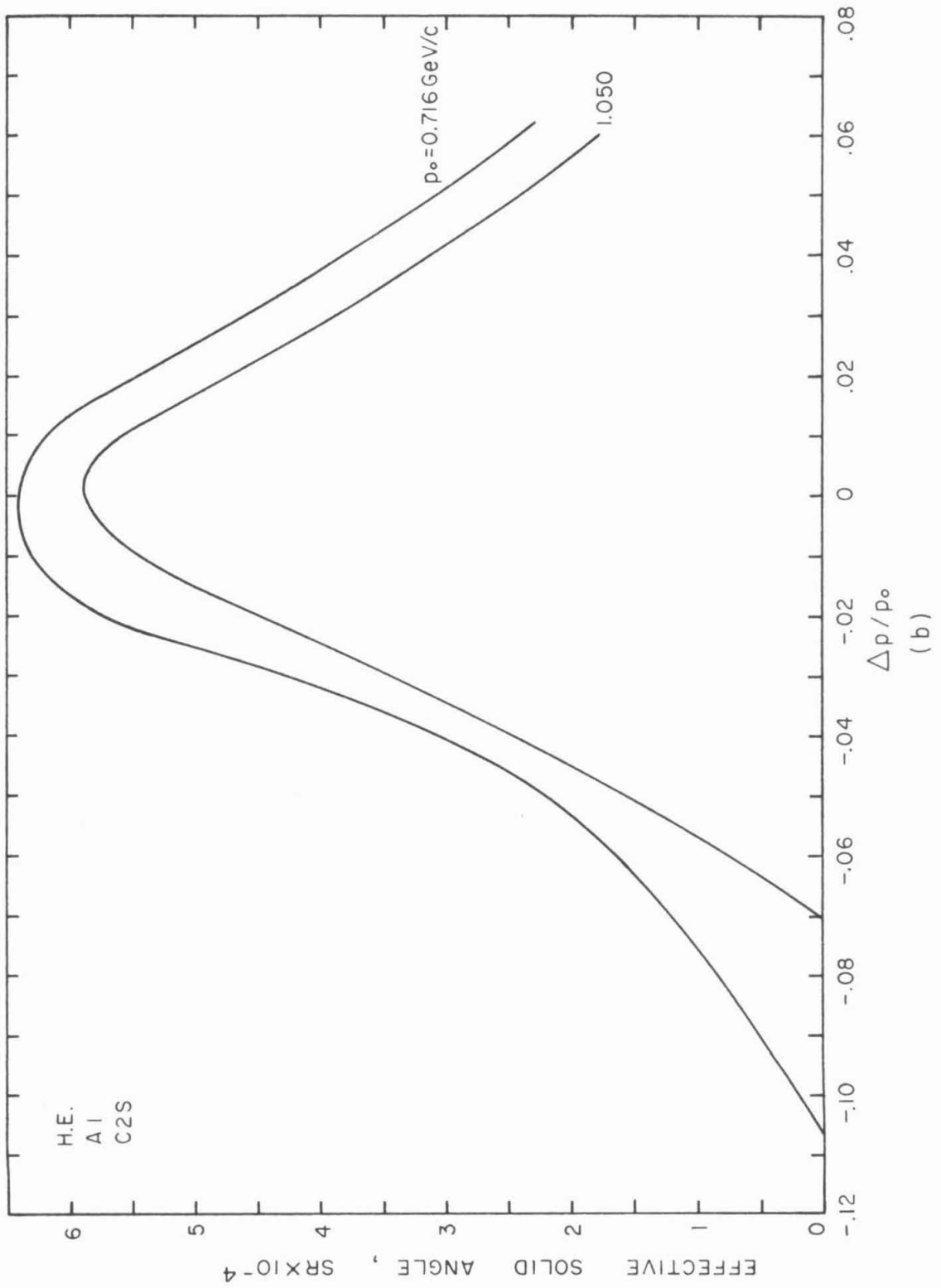
Figure A4. Momentum Response for Muons
From the Pion Decay

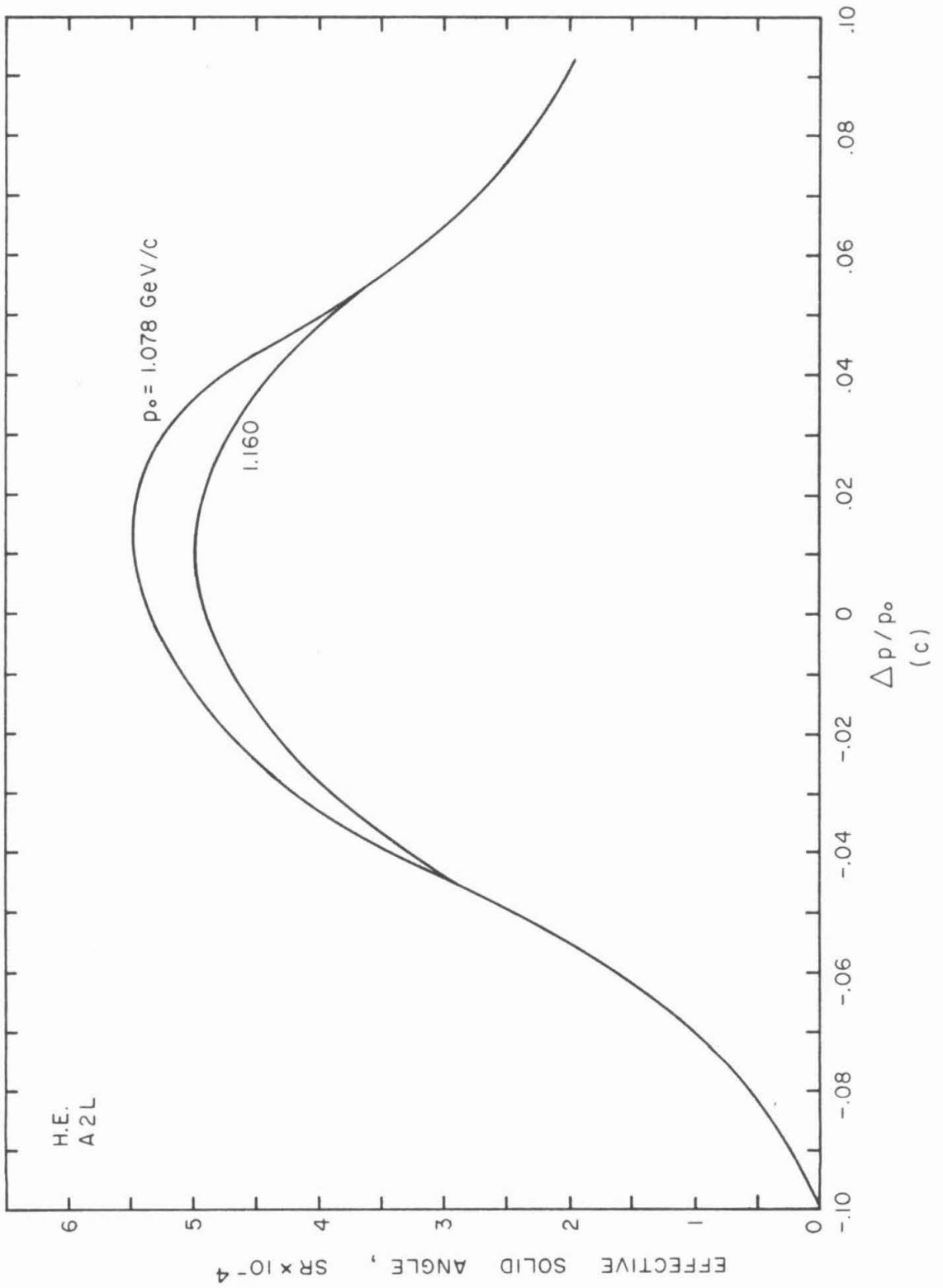
The abscissa is the fractional differences of the pion momentum from the central momentum, p_0 . ($\Delta p = p - p_0$)

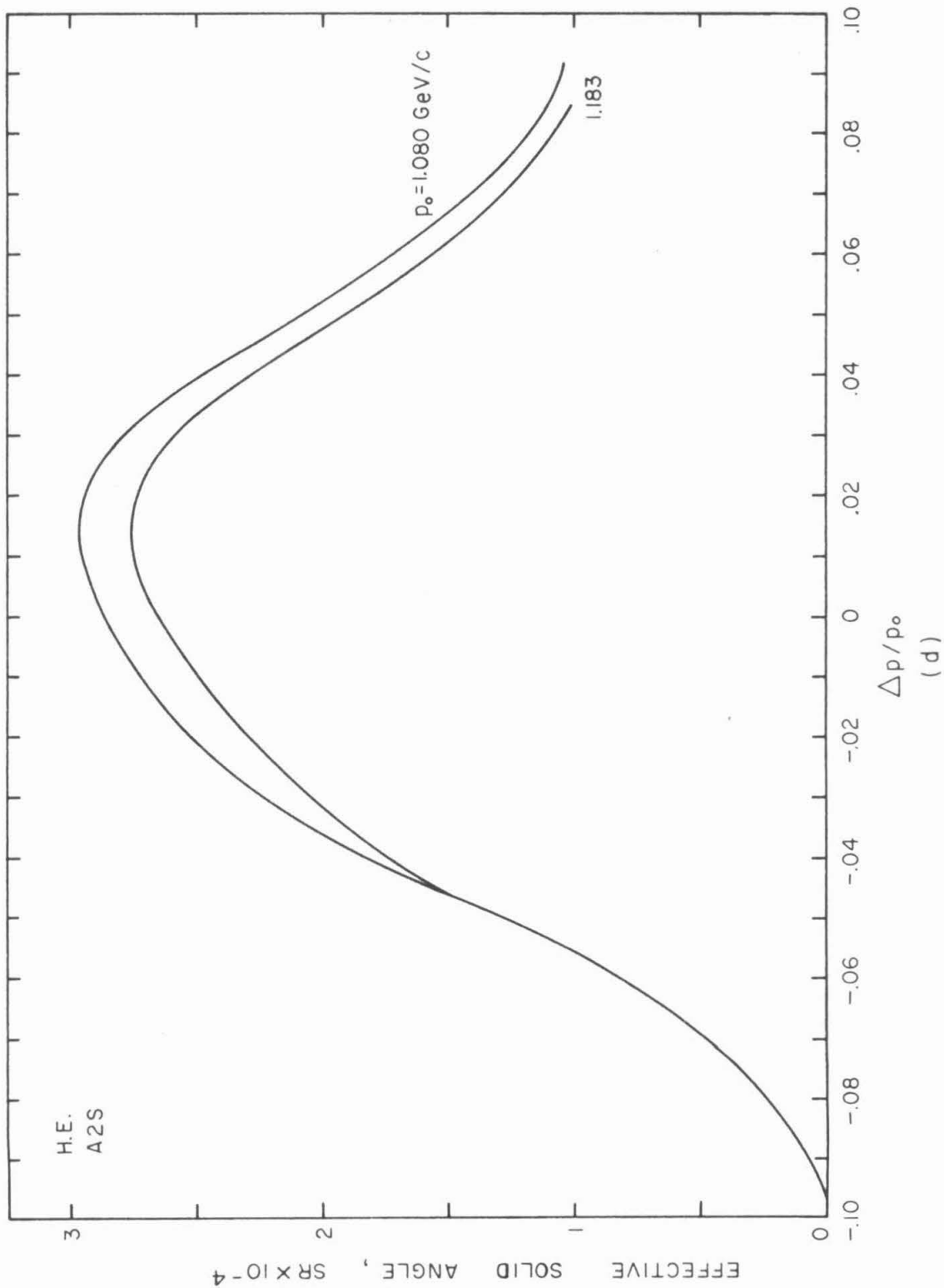
- (a) High energy magnet with the front aperture counter, A1, and the standard momentum defining counter, C2L.
- (b) High energy magnet with A2 and the small momentum defining counter, C2S.
- (c) High energy magnet with the large rear aperture counter, A2L, and C2L.
- (d) High energy magnet with the small rear aperture counter, A2S, and C2L.
- (e) Medium energy magnet with A1 and C2S.

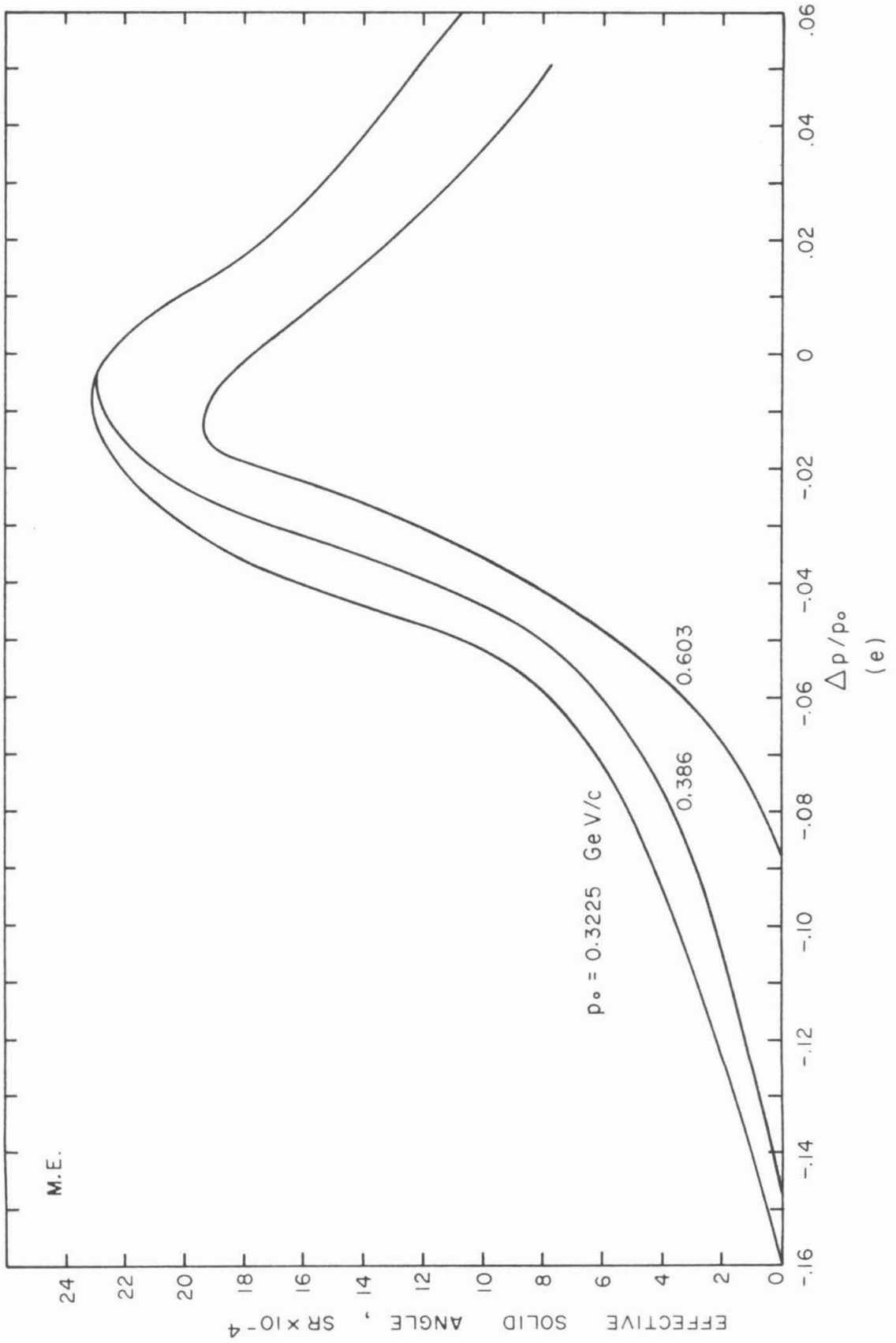
There are typically about twenty to forty points (not shown) for each curve with errors as in Figure A3.











lists the properties of the "scatterers" used in the calculation. Figure A5 gives the fractions of pions lost and gained due to scattering. For both the high energy and medium energy spectrometers the results were quite consistent with zero multiple scattering and thus no correction to the cross section was made. It should be noted that multiple scattering will tend to smear out the spectrometer resolution (in angle and momentum). However, this experiment is not very sensitive to this effect because of the well-behaved pion kinematics.

TABLE A2

Multiple Scattering Calculation Parameters

The first part of the table gives the radiation lengths in cm and densities in g/cc of the materials through which the pions pass.

(Scattering in the target or its walls is not considered.)

The second part gives the positions and effective thicknesses of the "scatterers" used in the calculation. X-INT and θ are respectively the x-intercept in cm and the angle in radians of the plane of the "scatterer" in the coordinate system shown in Figure A2. EFF.L. is the effective thickness of the "scatterer" in cm, and RAD.L. is the thickness expressed as a fraction of a radiation length.

TABLE A2
MULTIPLE SCATTERING PARAMETERS

MATERIAL	RAD. L.	DENSITY
AIR	37.7	0.001149
SCINTILLATOR (CH)	46.4	1.052
LUCITE (C ₅ H ₈ O ₂)	43.6	1.18

H. E. SCATTERERS

MATERIAL	X-INT.	θ	EFF. L.	RAD. L.
1 AIR	-212.7	0.0	128.5	0.00392
2 AIR	-84.2	0.0	128.5	0.00392
3 SCINT. (A1)	-22.5	0.05236	0.635	0.0144
4 AIR	0.0	0.61959	118.	0.00360
5 SCINT. (A2)	0.0	1.259	1.651	0.0281
6 AIR	147.0	0.47619	125.	0.00381
7 AIR	288.0	0.47619	125.	0.00381
8 SCINT. (C1)	356.4	0.47619	2.00	0.0455
9 LUCITE (C)	367.9	0.47619	3.81	0.1030

M. E. SCATTERERS

MATERIAL	X-INT.	θ	EFF. L.	RAD. L.
1 AIR	-87.0	0.0	68.	0.00207
2 AIR	-24.5	0.0	68.	0.00207
3 SCINT. (A1)	5.6	0.07854	0.635	0.0144
4 AIR	0.0	1.02102	110.	0.00335
5 AIR	152.	0.87324	65.	0.00198
6 AIR	254.	0.87324	65.	0.00198
7 SCINT. (C1)	304.7	0.87324	2.00	0.0455

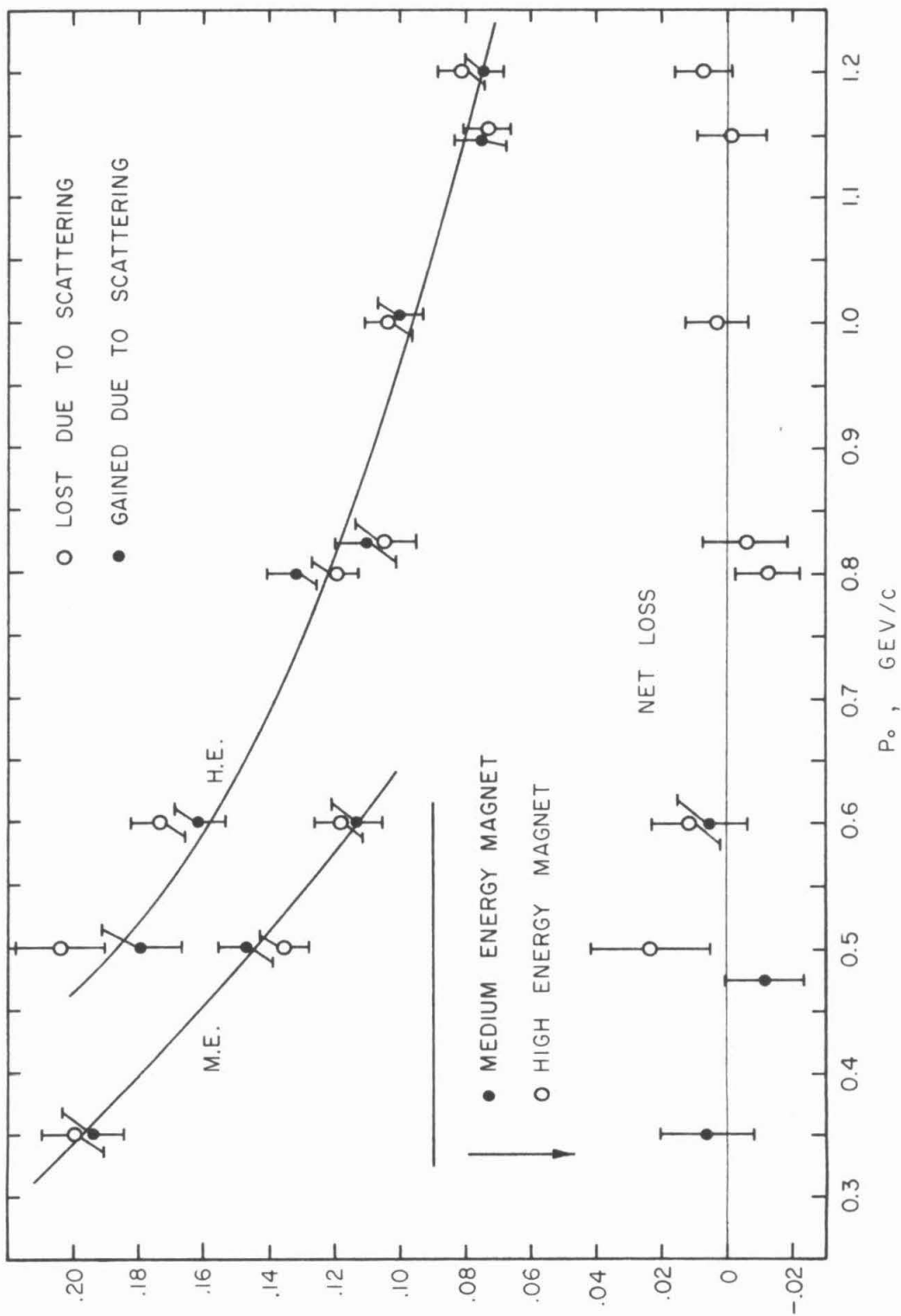


Figure A5 Multiple Scattering of Pions

APPENDIX IV EQUIPMENT CHECKS

Throughout the course of this experiment a number of measurements were made to test the satisfactory operation of the equipment. The results of these measurements are reported in this appendix.

1. A number of the points were measured using different magnet configurations. From these and a special measurement made when changing from the high to medium energy configuration the ratios of the spectrometer acceptances, $(\Delta\Omega \Delta p/p_0)$, for several configurations were obtained. In table A3 the spectrometer acceptances are listed along with the experimental and calculated ratios. The agreement is quite consistent with the statistical errors of the measurements.

2. The medium energy magnet was set at $\theta_{\text{LAB}} = 104.2^\circ$ and $p_0 = 0.4273 \text{ GeV}/c$ corresponding to $k_0 = 1.1 \text{ GeV}$. The end point energy of the bremsstrahlung beam, E_0 , was varied and the counting rates shown in Figure A6 were measured. The curve shown was calculated using the momentum response function calculated by the decay correction program (see Figure A3). The agreement between p_0 and E_0 is consistent to within the sensitivity of the measurement, as may be recognized from the fact that the measured points are not shifted consistently to either side of the curve. The consistency is within about 1% in p_0 and about 3% in E_0 .

3. The counting rates (full target minus background) were measured for three points previously measured by Dixon (5). Correcting

TABLE A3
The Spectrometer Acceptance

A. Spectrometer Acceptances.

Configuration	$\Delta\Omega \Delta p/p_0$ $\times 10^{-4}$	Source	$\Delta\Omega \Delta p/p_0$ from π - μ Decay Program $\times 10^{-4}$
H.E. A1 C2L	1.954	Dixon	2.14 \pm 0.03
H.E. A1 C2S	0.865	Dixon	0.91 \pm 0.03
H.E. A2L	1.08	Boydén	1.14 \pm 0.03
H.E. A2S	0.54	Boydén	0.59 \pm 0.03
M.E. C2S	2.75	Dixon	2.60 \pm 0.04

B. Acceptance Ratios.

Ratio	Calculated	Experimental
(H.E. A2S) / (H.E. A2L)	0.50	0.48 \pm 0.03
(H.E. A2L) / (H.E. A1 C2L)	0.552	0.59 \pm 0.04
(H.E. A1 C2S) / (H.E. A1 C2L)	0.442	0.43 \pm 0.03
(M.E. C2S) / (H.E. A1 C2L)	1.41	1.45 \pm 0.04

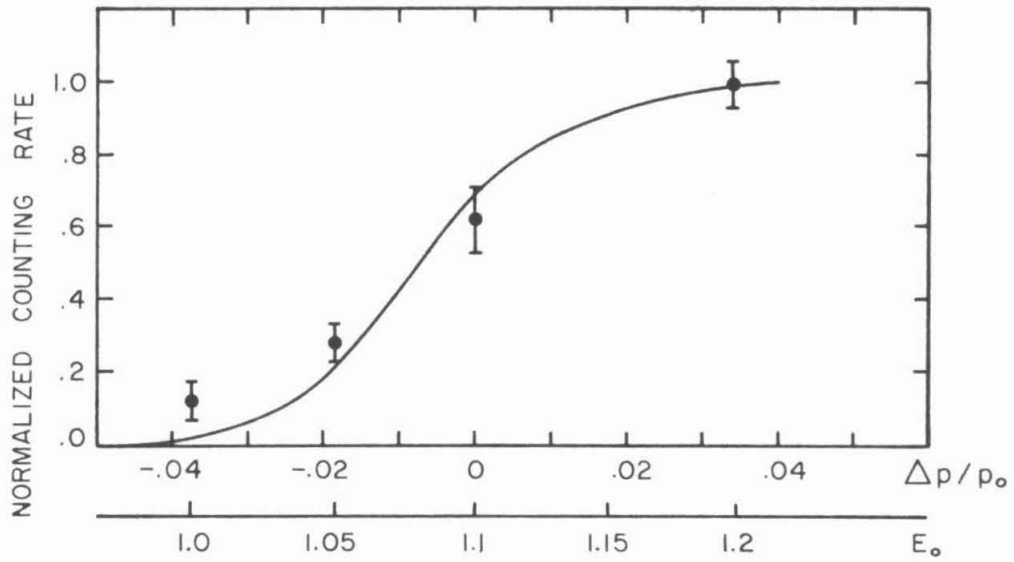


Figure A6. Measured and Calculated Spectrometer Response

for the different beam monitors used, the following comparison may be made:

E_0	θ_{LAB}	Dixon	This Exp.
1.08	26.1	0.96 \pm .05	0.90 \pm .05
1.08	35.7	0.61 \pm .04	0.62 \pm .04
1.00	17.6	0.84 \pm .06	0.89 \pm .05

To within the accuracy of these measurements (about 6%) the two sets of measurements are consistent.

4. Two tests were made with the field of the magnetic spectrometer reversed so that only negatively charged particles could be counted. The first was a search for electrons produced in the liquid hydrogen at a lab angle of 16.2° and at a momentum of 1.036 GeV/c (the $k = 1.1$ GeV, $\theta = 30^\circ$ point). The value of C_π obtained with the full hydrogen target was 0.0200 ± 0.0015 counts/BIP, while $0.0201 \pm .0019$ counts/BIP were obtained with the hydrogen removed, giving a net value of $-0.0001 \pm .0024$ counts/BIP. C_π was calculated using the formula which does not take account of the presence of electrons, so it may be concluded that there is not an appreciable number of electrons at this angle and momentum originating in the hydrogen. By comparison the positive-field π^+ counting rate is 0.60 counts/BIP. The observed counting rate is very likely due to negative pions produced in the target walls.

5. The second negative field test was made at a lab angle of 2.68° and a momentum of 1.084 GeV/c (the $k = 1.1$ GeV, $\theta = 5^\circ$ point), where there are many electrons produced. If the electron detection system

operates correctly the net counting rates should be zero. The net counting rates, C_{π^-} , are $-0.006 \pm .010$ for the double converter and $0.017 \pm .022$ for the single converter, both consistent with zero. The total counting rate, C , was approximately 1.7 counts/BIP while the positive-field π^+ counting rate, C_{π^+} , was approximately 0.17 counts/BIP.

APPENDIX V

BEAM MONITORING AND THE BREMSSTRAHLUNG SPECTRUM

The photon beam was monitored by a thick-walled sealed copper ionization chamber filled with a mixture of argon and CO_2 . This was periodically calibrated against a Cornell type quantometer (15), which served as the basic reference. With the spectrometer set at angles smaller than 15° the magnet yoke intercepted the beam, and it was necessary to use the thin-walled air ionization chamber located near the primary collimator. This chamber was sensitive to atmospheric changes, and so it was calibrated against the thick-walled chamber on the order of once an hour when data was being taken at small angles.

The charge on the ion chamber collector plates was integrated and recorded in units called BIPS (Beam Integrator Pulses) by integrator number 0249, which has an integration constant of 0.2110 microcoulombs per BIP. From a knowledge of the photon spectrum shape and the ion chamber calibration the number of BIPS could be converted into the number of photons in the energy range being used.

The ion chamber calibration was found to vary slowly with time. It is given for the data accumulation period of this experiment in Figure A7. The curves at the higher energies have been extrapolated from lower energy, with resulting larger errors. However, this error is still small compared to the statistical errors of the data.

With the synchrotron operating at $E_0 = 1.5$ GeV the R.F. accelerating system was not capable of accelerating all of the electrons to the peak energy. Therefore many struck the radiator at lower energies

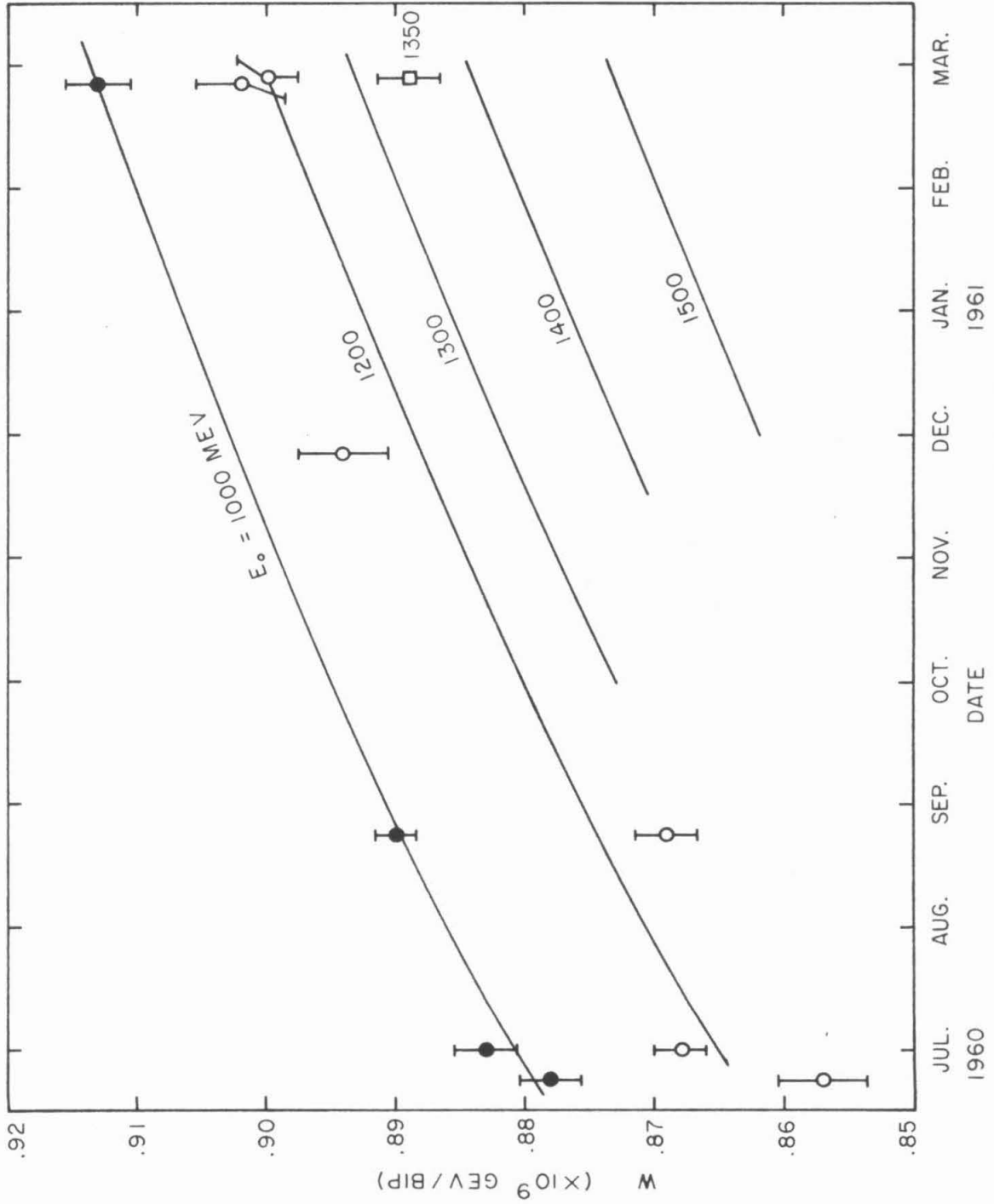


Figure A7. The Beam Monitor Calibration

thereby altering the spectrum shape. Moreover the number of electrons reaching 1.5 GeV varied from pulse to pulse with about one third reaching this energy on the best pulses. To maintain a constant spectrum, the counting electronics and the beam monitor output were gated so as to accept only those photons produced by 1.5 GeV electrons. To correct for the slight inaccuracy introduced by this procedure, W was multiplied by 0.97 ± 0.01 .

The bremsstrahlung spectrum, $B(k, E_0)$, has been given by Boyden (6). It is plotted in Figure A8.

Running concurrently with this experiment (and using the same photon beam) were the experiments of Ruderman (8) and Chang (7). Often the targets for these experiments were in the beam while data for this experiment was being taken. A simple calculation using the curve on p. 84 of High Energy Particles by Rossi (16), shows that for a 0.1 radiation length lead absorber the shape of the photon spectrum is virtually unchanged. Therefore no correction for material in the beam was made.

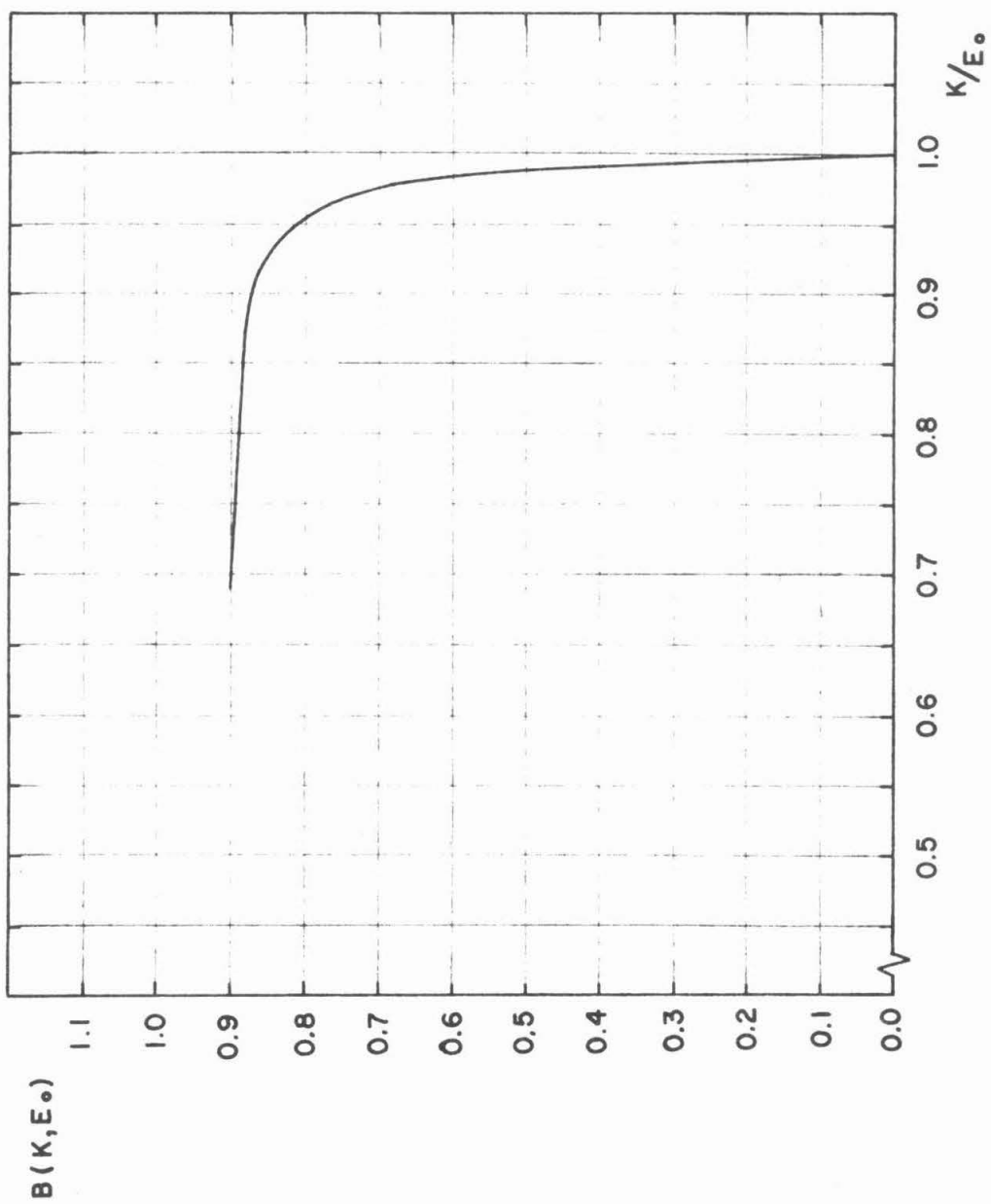


Figure A8. The Bremsstrahlung Spectrum

REFERENCES

1. H. Yukawa, Proc. Phys. -Math. Soc. Japan 17, 48 (1935).
2. Lattes, Occhialini, and Powell, Nature 160, 453 (1947).
3. B. Gregory, CERN Conference (1962).
4. Chew, Goldberger, Low, and Nambu, Phys. Rev. 106, 1345 (1957).
5. F. P. Dixon, Ph. D. Thesis, California Institute of Technology (1960).
F. P. Dixon and R. L. Walker, Phys. Rev. Letters 1, 458 (1958).
6. J. H. Boyden, Ph. D. Thesis, California Institute of Technology (1961).
7. T. Chang, Ph. D. Thesis, California Institute of Technology (1962).
8. H. Ruderman, Ph. D. Thesis, California Institute of Technology (1962).
9. P. L. Donoho, "A Magnetic Spectrometer for Analysis of Particles of Momentum up to 1200 Mev/c." (1957), Unpublished.
10. M. J. Moravcsik, Phys. Rev. 104, 1451 (1956).
11. J. G. Taylor, M. J. Moravcsik, and J. L. Uretsky, Phys. Rev. 113, 689 (1959).
12. L. Hand and C. Schaerf, Phys. Rev. Letters 6, 229 (1961).
13. J. Kilner, "A Computer Program for the Analysis of Pion Photoproduction Data." California Institute of Technology Synchrotron Laboratory Report CTSL-37 (1962).
14. G. Höhler, K. Dietz, and A. Müllensiefen, Nuovo Cimento 21, 187 (1961).
15. R. R. Wilson, Nuclear Instruments 1, 101 (1957).
16. B. Rossi, High Energy Particles, Prentice-Hall Inc., New York (1952).